Lumbar Spinal Injury Under Dynamic Compression

by

Maria Andreina Ortiz Paparoni

Department of Biomedical Engineering
Duke University

Date:_____

Approved:

_____
Cameron Dale R Bass, Supervisor

_____
Roger W. Nightingale

_____
Brenton Hoffman

_____
Frank A. Pintar

_____
Kerry A. Danelson

Dissertation submitted in partial fulfillment of
the requirements for the degree of Doctor
of Philosophy in the Department of
Biomedical Engineering in the Graduate School
of Duke University

2022

ABSTRACT

Lumbar Spinal Injury Under Dynamic Compression

by

Maria Andreina Ortiz Paparoni

Department of Biomedical Engineering
Duke University

Date:_____

Approved:

_____
Cameron Dale R Bass, Supervisor

_____
Roger W. Nightingale

_____
Brenton Hoffman

_____
Frank A. Pintar

_____
Kerry A. Danelson

An abstract of a dissertation submitted in partial fulfillment of the requirements for the degree of Doctor of Philosophy in the Department of Biomedical Engineering in the Graduate School of Duke University
2022

Abstract

Spinal trauma is a major issue with considerable societal, economic, and physical consequences. Lumbar spine injuries during dynamic compression have been highly prevalent in recent American military conflicts in part due to the increased use of improvised explosive devices. The susceptibility of the lumbar spine during these scenarios can reduce functional capacity of soldiers and result in disability and morbidity in the military population. Characterizing the spine response during dynamic compression scenarios is essential in understanding injury risk in military personnel from underbody blast. Further, translating the experimental response to real world applications is crucial in developing future vehicle designs and mitigation strategies to reduce the incidence of these injuries.

To advance the understanding of lumbar spine injury tolerance an axial loading lumbar spine vertebral body fracture injury criterion (L_{ic}) across a range of three postures was established from 75 tests performed on instrumented cadaveric lumbar spine specimens. The spines were predominantly exposed to dynamic axial compressive forces from an upward vertical thrust with 64 of the tests resulting in at least one vertebral body fracture and 11 in no vertebral body injury. A loglogistic parametric survival analysis determined that the tolerance of the lumbar spine was 5569 N, 4618 N, and 4493 N for the tested nominal, pre-flexed, and pre-extended postures respectively. The differences in

tolerance across the tested posture suggests that the injury probability is not captured by axial data alone. Therefore, a combined loading injury criteria was developed to provide an improved assessment.

The susceptibility of the lumbar spine during underbody blast loading scenarios could also be exacerbated by coupled moments that act with the rapid compressive force depending on the occupant's seated posture. The influence of the bending moment on the injury tolerance of the lumbar spine was evaluated using a combined metric that considers both the axial force and bending moment of the loading event. This combined loading lumbar spine vertebral body fracture injury criterion (CL_{ic}) across a range of postures was established from 75 cadaveric lumbar spine tests. The proposed CL_{ic} utilizes a metric (κ), based on prismatic beam failure theory, resulting from the combination of the T12-L1 resultant sagittal force and the decorrelated bending moment with optimized critical values of $F_{r,crit}$ = 5824N and $M_{y,crit}$ = 1155Nm. The 50% risk of lumbar spine vertebral body fracture corresponded to a combined metric of 1, with the risk decreasing with the combined metric value. At 50% injury risk the Normalized Confidence Interval Size improved from 0.24 of a force-based injury reference curve to 0.17 for the combined loading metric.

At this point the injury tolerance for the lumbar spine during UBB events to the axial force and a combined loading metric was investigated for a limited range of occupant's seated postures. However, it is highly desirable to expand the criterion to

consider postures and dynamically evolved positions for a wider range of compression and bending moments in the lumbar spine. Therefore, the established lumbar combined injury criterion (CL_{ic}) was expanded to a wider range of initial and dynamically evolved postures and account for a higher contribution of the bending moment to the loading scenario. An expanded combined loading injury criterion (ECL_{ic}) was developed by testing an additional 15 specimens for initial and dynamically evolving postures that further increased the extension or flexion of the lumbar spine. These were combined with the 75 previously tested specimens in the nominal posture range. The injury criterion established from 90 cadaveric tests, produced a resultant sagittal force and decorrelated bending moment critical values of $F_{r,crit}$ = 6011N and $M_{y,crit}$ = 904 Nm. Out of the 90 specimens tested 77 had at least one vertebral body fracture, with 13 specimens having minor injuries or no injuries. The 50% risk of lumbar spine vertebral body fracture was normalized to a combined metric of 1, with the risk decreasing with the combined metric value.

Finally, translating cadaver injury risk to equivalent anthropometric test devices measurements is a vital step for effective injury mitigation efforts. The commonly used matched-pair approach to translate these data consistently overestimates dummy injury risk, which then exaggerates human injury tolerance. A novel translation method based on energy equivalency was proposed to avoid these errors by matching strain energy between cadaver and dummy. To translate a single metric, say force, to an ATD risk

assessment (IARC), the force-energy responses for both cadaver and simulated dummy measurements were used to determine the transfer function from cadaver measurement to ATD measurements at iso-energy. Similarly, a generic a combined metric, similar to the combined loading injury criterion (CL_{ic}) developed, was used to illustrate the translation of a complex loading scenario by characterizing the energy response of both cadaver and ATD in the corresponding force/moment duplets that define the CL_{ic}.

Dedication

Para el amor de mi vida, Fede.

Contents

Abstract iv

Dedication viii

List of Tables xii

List of Figures xiv

Acknowledgements xvi

1 Introduction 1

1.1 Objectives 4

1.2 Specific Aims 6

1.2.1 Evaluate the human lumbar spine axial force tolerance for a nominal range of occupant postures to underbody blast loading scenarios. 6

1.2.2 Propose an injury metric that accounts for the influence of the bending moment on the injury tolerance of the lumbar spine for underbody blast loading scenarios. 7

1.2.3 Expand the applicability of the proposed combined loading injury criterion by incorporating a wider range of postures to the analysis of the injury metric. 8

1.2.4 Develop a methodology to translate the developed injury criteria to an anthropometric test device maintaining equivalent injurious conditions. 8

2 Lumbar Spine Injury Criterion: Axial Loading 10

2.1 Introduction 10

2.2 Materials and Methods 11

2.2.1 Specimen preparation, testing and signal processing 12

2.2.2 Injury Probability: Parametric Survival Analysis 17

2.2.3 Injury Censoring 18
2.3 Results 19
2.3.1 Injury Censoring 23
2.3.2 Injury Probability 25
2.4 Discussion 29
3 The Combined Loading Injury Criterion 33
3.1 Introduction 33
3.2 Materials and Methods 34
3.2.1 Moment decorrelation 34
3.2.2 Lumbar Injury Criteria: combined loading 36
3.3 Results 38
3.3.1 Moment decorrelation 38
3.3.2 Combined loading injury criterion (CL_{ic}) 41
3.4 Discussion 46
4 Expansion of the Combined Metric 52
4.1 Introduction 52
4.2 Materials and Methods 53
4.2.1 Combined metric optimization 57
4.2.2 Alternative weightings for the expanded range data 58
4.3 Results 58
4.3.1 Moment decorrelation 60
4.3.2 Expanded combined loading metric 62

4.3.3 Alternative weighting 64
4.4 Discussion 66
5 The Energy Method 70
5.1 Single metric translation 71
5.2 Combined loading metric translation 78
6 Conclusions 81
6.1 Contributions and Impact 82
6.2 Future work 84
Appendix A 86
References 93
Biography 99

List of Tables

Table 2-1: Injury outcome for first 20 specimens of the test series. 22

Table 2-2: Injury metric values at the T12/L1 IVD center for first 20 specimens of test series. 24

Table 2-3: Anderson-Darling coefficients for three assessed distributions. 25

Table 2-4: Selected injury risk values of axial force (F_z) for lumbar specimens subjected to dynamic compression in the nominal posture. 26

Table 2-5: Selected injury risk values of axial force (F_z) for lumbar specimens subjected to dynamic compression in the pre-flexed posture. 27

Table 2-6: Selected injury risk values of axial force (F_z) for lumbar specimens subjected to dynamic compression in the pre-extended posture. 27

Table 3-1 Anderson-Darling (AD) coefficient for each distribution parametric distribution. 41

Table 3-2: Selected CL_{ic} values for the T12-L1 Resultant Force (Fr) and Bending Moment (My) Combination Metric 43

Table 3-3: Selected range of IRC values for the T12-L1 Resultant Force (F_r) for Duke's data set 45

Table 3-4: . Selected IRC values for the T12-L1 Resultant Force (F_r) for MCW's data set. 45

Table 4-1: Injury outcome from the 15 specimens of the expanded posture test series. ... 59

Table 4-2: Summary of combined Fr and Fz based peak values from expanded test series. 60

Table 4-3: Optimized Anderson-Darling (AD) coefficients for the parametric distributions evaluated. 62

Table 4-4: Selected injury risk values for the T12-L1 resultant force and moment combined loading metric (λ). 63

Table A.-1: Input conditions and injury description summary for cadaver tests used in L_{ic} and CL_{ic} generation. 86

Table A-2: Summary of combined F_z, M_y, and F_r based peak values from Duke and MCW thoracolumbar data set for L_{ic} and CL_{ic} generation. 90

List of Figures

Figure 2-1. Lumbar spine posture derived from the Seated Soldier Study 14

Figure 2-2: Duke experimental setup for a nominal extended specimen (LSPN19)..... 15

Figure 2-3: Sagittal microCT images depicting injuries carried out during pre-flexed testing. 20

Figure 2-4: Sagittal microCT images depicting injuries carried out during pre-extended testing. 21

Figure 2-5: Example of fracture initiation determination for lower bound of censoring interval for Duke test LSPN31..... 23

Figure 2-6: Human Injury Probability Curve (HIPC) for three postures under dynamic compression. 25

Figure 2-7: Normalized Confidence Interval Size (NCIS) for the axial loading metrtic for three tested postures:..... 28

Figure 3-1: Optimized moment arm (antero-posterior translation)..... 35

Figure 3-2: Combined loading stress and force failure criteria based on prismatic beam formulation. 37

Figure 3-3: Correlation of F_z and M_y for Duke and MCW lumbar tests. 39

Figure 3-4: Posterior translations of the estimated effective moment arm location that minimizes the correlation between F_z and M_y 40

Figure 3-5: Injury risk comparison of the lumbar spine during dynamic compression. .. 42

Figure 3-6: Normalized confidence interval size (NCIS) for combined loading metric of integrated data set..... 44

Figure 4-1: Expanded range of postures based on seated soldier. 55

Figure 4-2: Test setup for LSPN36. 56

Figure 4-3: Correlation of Fz and My for 15 expanded range Duke lumbar tests. 61

Figure 4-4: Posterior translations to the effective center of rotation that minimize correlation between F_z and M_y for the expanded data set. 61

Figure 4-5: Lumbar spine vertebral body fracture injury risk for the expanded range of postures. 63

Figure 4-6: Anderson-Darling fit coefficients for various distribution and weighting values for F_z and F_r based injury risk models. 64

Figure 4-7: NCIS values for Loglogistic distribution for F_z and F_r based injury risk models. 65

Figure 4-8: Loglogistic injury risk for 1x and 5x weigthing. 65

Figure 5-1: Linear elastic scaling at equal force. 72

Figure 5-2: Linear elastic scaling at equal displacement. 73

Figure 5-3: Linear elastic isoforce equivalency method on generic dataset for HIPC to IARC translation. 74

Figure 5-4: Force-Energy response and injury risk curve through the commonly used matched-pair method. 75

Figure 5-5: Scaling for a linear elastic model at iso-energy. 76

Figure 5-6: Linear elastic iso-energy equivalency of cadaver and ATD response on generic dataset. 77

Figure 5-7: Cadaver to ATD transfer function at iso-energy for a generic dataset. 77

Figure 5-8: Example of surface plot of Force (F_z or F_r) and Moment (M_y) vs. Energy for cadaver energy response extrapolation. 80

Acknowledgements

A lot of people have been involved in the successful completion of this dissertation and I will be forever grateful to all of them.

To start I would like to thank my advisor, Dale Bass. His support, thoughtful (and always interesting conversations), and life lessons have been invaluable in my journey. There are countless reasons why I consider myself fortunate to be a part of his lab, but I am especially grateful that he entrusted me with such an important and complex project, which has allowed me to become the well-rounded biomechanist that I am today. I would also like to thank Roger Nightingale for his support and long conversations on spine biomechanics, buckling events, and spinal injury; having a world expert just down the hall was vital in understanding the immensely complex system that is the human spine. To my committee members, Frank Pintar and Kerry Danelson, I will be forever grateful for all the knowledge you imparted during the countless project calls and meetings and your contributions to this project, I have been truly privileged to learn from the best. I am also thankful to Brent Hoffman, from his great disposition and contributions during the course of my project and for giving me the opportunity to teach my first college class in biomechanics.

To my friends at the Injury Biomechanics Lab. I was so fortunate to be "sandwiched" across two generations of bright and incredible researchers! Thank you for the countless hours of testing, for the camaraderie, the support, the lunches, and scientific

and cultural teachings. I would like to thank the mentors that became my friends, Allison Schmidt, Jay Shridharani, Brian Bigler, Courtney Cox, Allen Yu, Rachel Lance, and Hattie Cutcliffe; I will always treasure all the lessons that you taught me and the ones we had to figure out together. To the "younger" generation of the Bass lab, Chris Eckersley, Joost Op 't Eynde, Connie Morino, and Mitchell Abrams; thank you for the spinal injury parties, from necropsies, and testing to watching high-speed videos of fractures over and over. Not only did you make important scientific contributions, but you made the dauting tasks truly enjoyable, thank you for being so supportive during the "crazy times" and for always be willing to navigate complex scientific problems, even if it meant hours of zoom calls. To Jason Kait, thank you for becoming the best testing partner and a great friend. I was always so impressed with your ingenuity and handiness during testing, thank you for sharing some of that with me and for teaching me a thing or two about testing, engineering, and life. To Jason Luck, thank you for bringing me in to the lab as a mechanical engineer Master student that knew little of biomechanics. Thank you for introducing me to experimental testing and guiding me through the challenging work we perform in our lab, having you in my corner has been both reassuring and crucial when sorting out the difficulties along the PhD journey. I would also like to thank all our Master of Science students, in particular Michaela Pigue and Rhylee DeCrane, thank you for all your contributions to my project; your cheerful disposition, eager desire to learn, trust in my capabilities, and dedication were invaluable. Finally, I would like to acknowledge the

unsung hero of the Bass Lab, Kathy Bass. Thank you for your hospitality, for receiving us in your home, for making sure we had a bed to sleep in during all our travels and for always finding a way back home for us, even when our flights got cancelled.

A mi familia,

No hay palabras suficientes que puedan describir lo agradecida y orgullosa que me siento de tener un núcleo familiar tan amplio, tan amoroso y que ha proveído tanto apoyo a lo largo de todos estos años. A mis padres, Maria Nelly y César José, gracias por enseñarme el significado de la dedicación y el trabajo duro. Ustedes siempre han sido mi ejemplo a seguir y fuente de inspiración, gracias por darlo todo por sus hijos y por brindarnos las increíbles oportunidades que hoy nos han permitido convertirnos en quienes somos. A mis hermanos, César Alejandro y Francisco Javier, gracias por su apoyo incondicional, por su amistad, por las enseñanzas que me dieron y las que tuvimos que descubrir juntos. A mi segunda madre, Gladys; decir gracias por todo no expresa lo afortunada que me siento de tenerte en mi vida. Gracias por dejarlo todo solo para visitarme y para apoyarme en mis momentos más difíciles. Gracias por toda tu ayuda en trabajos y proyectos; y al igual que mis padres, gracias por enseñarme lo que significa ser un ingeniero dedicado y brillante! A todos mis tíos y primos, gracias por todo el cariño y apoyo a lo largo de estos años. Crecer rodeada de un ambiente tan amoroso, solidario, divertido y comprensivo ha sido vital para convertirme en la persona que soy hoy.

Finalmente, a los más importantes de todos: mi esposo Fede y mis niños Nova y Capi. Me quedo sin palabras para expresarles lo que significan para mí. Ustedes son mi todo, son la razón de mi alegría y mi fortaleza. Gracias a ustedes he aprendido a amar más allá de lo que pensaba posible. Me han enseñado el significado de formar una familia y un hogar. Navegar el PhD junto a ustedes ha sido una aventura única en nuestras vidas y no puedo esperar a ver cuál será la siguiente. Cualquiera que ella sea, sé que con ustedes a mi lado seguiremos superando los obstáculos que se nos presenten, pero más importante disfrutaremos de todas las alegrías que nos depara nuestro futuro. Los amo con todo mi corazón!

1 Introduction

The lumbar spine is an important site of injuries during high-rate under-seat loading scenarios where injuries, such as bony fractures and ligamentous disruptions, can often lead to spinal cord damage (Arsh et al., 2017). Particularly, modern changes in warfare have shown the increased use of explosive devices in concert with ubiquitous use of vehicles for increased mobility that has led to an increasing number of underbody blast (UBB) injuries (Bailey et al., 2015; Kang et al., 2012; Spurrier et al., 2016). These events occur when an explosive, typically an improvised explosive device (IED), detonates from below a ground vehicle. Previous generations of U.S. military vehicles were not specifically designed to protect soldiers from these large underbody blasts, and current and future vehicles need objective assessment techniques to limit injury potential (Spurrier et al., 2016; Vasquez et al., 2018). Lumbar spine fractures rank as the fourth most frequent Abbreviated Injury Scale (AIS) 2+ injury for service members wounded from underbody blast and second among those killed in action (Loftis et al., 2019). Of those wounded in action from UBB, 19% and 35% suffered from a cervical and lumbar spine injury respectively (Vasquez et al., 2018). Soldiers with spinal injury due to blast from 2003-2008 spent an average of 5.84 days in the ICU and 10.48 days in the hospital (Szuflita et al., 2016). Beyond acute physical disability, sequelae leading to chronic back pain can negatively influence mental health and reduce overall quality of life (Groessl et al., 2017; Kovacs et al., 2004; Manchikanti et al., 2002).

Recognizing the lumbar spine as an important site of injuries during high-rate under-seat loading scenarios (Danelson et al., 2018), it is critical to develop an injury criterion better suited to evaluate UBB events. Data used to derive civilian automotive injury criteria differ from an UBB event in loading rate, injury patterns, and loading profile (Danelson et al., 2015). These differences limit the ability of currently established automotive criteria of informing injury metrics to develop protection systems or measures that could mitigate an UBB related injury. The lumbar spine anatomy can be particularly vulnerable to injuries in this scenario due to the rapid compressive loading of the spine components. Further, the occupant's seated posture and weight distribution can result in the coupling of the compressive force with bending moments that can influence the injury risk.

Vertical loading contributes to the overall loading of the spine during underbody blast events (Vasquez et al., 2018; Yoganandan et al., 2013; Yoganandan et al., 2020b). Yoganandan et al. developed an injury risk criterion considering the axial and resultant force on the spine as the primary contributor to injury (Yoganandan et al., 2020b). However, this previous study did not account for the bending response of the lumbar spine. Given the complex geometry and loading path during UBB, the position of the spine will not necessarily be in line with the loading direction in the instant that the underbody force loads the pelvis. Further, the spine will likely dynamically evolve into complex orientations that have different local contributions from axial/shear forces and

bending moments. So, the loading pattern exhibited during high-rate compression events is not captured by axial force data alone. Available studies have yet to broadly consider the effect of combined loading of the spine during UBB which can lead to an underestimation of the bending moment influence on injury outcome. A combined injury criterion considering both axial forces and bending moment can expand the assessment of injury risk and can ultimately lead to the safety of future vehicles or mitigation strategies to reduce the incidence of spinal injuries during UBB.

Since the 1970s, injury assessment reference values (IARVs) and injury assessment reference curves (IARCs) have been widely used in multiple applications such as the enhancement and development occupant restraint systems, anthropometric test devices, airbag systems, policy regulation, and retrospective analysis of injuries in the field, among other applications (Foster et al., 1994; Mertz et al., 1989; Mertz et al., 1991; Mertz et al., 1996; Nightingale et al., 1997; Nyquist et al., 1980; Yoganandan et al., 1996). Such injury assessments are based on studies that have directly defined human injury tolerance values from cadaveric, animal, volunteer, and real-world injury rates to inform anthropometric test device(s) (ATD) performance requirements (Eppinger et al., 1998; Mertz et al., 1997; Nightingale et al., 1997; Pintar et al., 1989; Prasad and Daniel, 1984). To develop IARCs one widely used approach is the commonly used matched-pair testing where both the ATD and cadavers are evaluated under similar loading, boundary and initial test conditions often with an energy-based input such as a mass impacting with a defined

input velocity (Poplin et al., 2017). While this method allows the development of a direct correlation of measured ATD responses to cadaver injury outcomes, there are two areas that limit the effectiveness of this approach in developing IARCs. First, there are differences in stiffness between the ATD and cadaveric or animal surrogates. Second, the ATD is usually designed to remain intact under potentially injurious loading where the cadaver or animal may suffer fractures or failures that compromise available load bearing capacity. This effect limits peak forces and moments that may be developed in the cadavers or animals compared with the matched-pair ATD tests. This limitation of matched-pair testing will cause an overestimation of the injury risk estimates in ATDs compared with cadavers resulting in higher, less conservative, injury values. In general, injuries in humans, animals or cadavers occur under an initial velocity or impulse condition which results in an energy input, and local failure of biological tissue is usually associated with input strain energy. Therefore, using an energy equivalency method for the IARC generation can ensure that there are comparable testing and failure conditions between the cadaver and ATD despite the stiffness and performance differences across the two components.

1.1 Objectives

The objective of this work is to provide information that can be used in the development of injury mitigation tools and strategies to reduce the incidence or severity of underbody blast injuries to the lumbar spine.

Characterizing the injurious spine response under IED loading scenarios will be achieved by subjecting cadaveric human lumbar spine specimens to dynamic compression. Innovative acoustic techniques developed by the Bass lab (Shridharani et al., 2016; Shridharani et al., 2021) will be used as a complementary tool to provide further information on the presence of spinal injury. This technique, used in conjunction with methods such as evaluation of stiffness behavior, will improve specimen injury detection. Furthermore, by refining the determination of injury initiation with acoustic emissions we will inform the data censoring for the proposed injury criteria allowing to us to narrow on the range of expected injury. The proposed injury criterion will assess the injury tolerance of the lumbar spine to predominantly axial forces during the UBB scenario using tests restricted to initial postures around a nominal seated posture. Based on the data gathered for the axial injury criterion, an additional injury criterion will be developed incorporating a combined loading metric to add the effects of the antero-posterior bending moment on spinal failure. This capability is valuable in the risk assessment of both a restricted range of seated posture loading conditions and postures into which the lumbar spine can shift to during an UBB loading event. The methodology developed in the force/moment injury criterion remains approximately valid for a much wider range of forces and moments in the sagittal plane so additional experiments will be performed over a wider range of flexion/extension of the spine will be investigated and incorporated to expand the injury criterion. Finally, we propose an innovative iso-energy approach for

IARCs generation that will ensure that the testing conditions between the cadaver and the ATD are comparable despite the differences in stiffness and behavior across the two components, allowing to remove these two confounding factors from the ATD injury assessment.

1.2 Specific Aims

To accomplish the aforementioned objectives, we plan to evaluate the axial force tolerance of the human lumbar spine under dynamic compression across three different initial seated postures that represent the mean and standard deviation values for a seated posture studied in a military age population. Further, we will assess the effect that the bending moment has on the injury tolerance by introducing a combined loading injury metric, which will later be extended across a wider range of occupant postures to capture the influence of higher bending moments during the loading event. Finally, we will propose a new methodology, based on energy equivalency, to translate the information derived from human cadaveric testing to real world applications.

To accomplish the objectives of this project the work will be divided into the following specific aims:

1.2.1 Evaluate the human lumbar spine axial force tolerance for a nominal range of occupant postures to underbody blast loading scenarios.

For this aim we will develop an axial loading injury criterion from cadaveric human testing by means of parametric survival analysis. To achieve our objective,

unembalmed human cadaveric lumbar spines will be subjected to injurious levels of predominantly dynamic compression to determine their fracture tolerance. Refinement of the injury initiation will be achieved by using acoustic emissions to provide a narrow range of censoring for the data set and improve the injury risk assessment. The successful completion of this aim will elucidate the injury tolerance of the lumbar spine in axial loading under an UBB event across a nominal range of postures.

1.2.2 Propose an injury metric that accounts for the influence of the bending moment on the injury tolerance of the lumbar spine for underbody blast loading scenarios.

For this specific aim we will develop a spinal fracture injury criterion for the lumbar spine under dynamic compression that incorporates a combined loading metric to account for the influences of the sagittal forces (superior-inferior compression and antero-posterior shear) and the sagittal bending moment on the injury outcome.

For this objective, a reanalysis of the previous human cadaveric tests will be performed to incorporate a combined loading metric that considers the effects of the bending moment. This will allow the expansion of the range of lumbar dynamic force/moment injury assessments for the military population. This capability becomes valuable in the risk assessment of both a restricted range of seated posture loading conditions and dynamic postures into which the lumbar spine can shift to during an UBB loading event.

1.2.3 Expand the applicability of the proposed combined loading injury criterion by incorporating a wider range of postures to the analysis of the injury metric.

For this aim additional human cadaveric lumbar spines will be tested in a wider range of initial occupant seated postures that evolve into an expanded range force/moment time histories compared with the previous predominantly axial tests. This will increase the contribution of the bending moment to the injury mechanism.

By accounting for the sagittal forces in the combined loading metric, the expansion of new postures can be incorporated into the same framework followed to develop the combined loading injury risk for the range of nominal postures. This expansion of combined loading metric will increase the applicability of the injury risk criterion to a wider range of seated occupant postures. This provides a more comprehensive injury assessment over different scenarios that can occur during an UBB event.

1.2.4 Develop a methodology to translate the developed injury criteria to an anthropometric test device maintaining equivalent injurious conditions.

The human injury probability curves (HIPCs) for the lumbar spine developed previously will be translated to an injury assessment reference curve for a generic anthropometric test device at iso-energy conditions. The cadaveric energy response to injurious conditions and a generic energy response dummy data set will be used to determine the transfer function from cadaver measurement to ATD measurement leading

to two demonstration ATD injury assessments, an axial loading t and a combined injury metrics.

The commonly used matched-pair approach used to develop injury assessment reference curves (IARCs) for ATDs from cadaveric testing faces two particular challenges: differences across the material properties and failure force/moment levels between a cadaver and an ATD. Direct pairing of tests with common energy inputs invariably causes an overestimation of the injury risk assessments in the ATD compared with cadavers. This produces higher, less conservative, injury assessments in the dummy. The proposed iso-energy methodology will ensure that the matching conditions between the cadaver and the ATD are comparable despite the differences in stiffness and failure performance across the two components, removing these two confounding factors from the ATD injury assessment.

2 Lumbar Spine Injury Criterion: Axial Loading

In this chapter an axial loading lumbar spine vertebral body fracture injury criterion (L_{ic}) across a range of postures was established from 75 tests performed on instrumented cadaveric lumbar spine specimens. The spines were exposed to predominantly dynamic axial compressive forces. One vertebral body fracture occurred in 64 of the tests. No vertebral body fractures were seen in 11 tests[1]

2.1 Introduction

During Operation Iraqi Freedom and Operation Enduring Freedom spine injuries accounted for 5.5% of all casualties, the highest incidence of spine injuries than any other American military conflict (Blair et al., 2012). Ground U.S. military vehicles were not initially designed to protect soldiers from large underbody blast forces (Vasquez et al., 2018). The incidence of AIS 2+ lumbar spine fractures ranked 4th amongst soldiers wounded in action and 2nd amongst soldiers killed in action (Loftis et al., 2019). Further, lumbar spine injuries can impact a warfighters' ability to carry out their field operations, and are frequently associated with lifetime disabilities that significantly impact quality of life after the injury (Craig et al., 1990; Possley et al., 2012).

---

[1]This chapter contains materials originally published in Annals of Biomedical Engineering: 49, 3018-3030 (2021). (DOI: https://doi.org/10.1007/s10439-021-02823-x) © 2022 Springer Nature Switzerland AG. Part of Springer Nature. This reuse is permitted under the publisher's copyright terms. Collaborators on this work are gratefully acknowledge. (Ortiz-Paparoni et al. 2021)

To contribute towards injury mitigation and the protection of soldiers the Warrior Injury Assessment Manikin (WIAMan) program (an Army-sponsored initiative) has been developing an advanced ATD that can capture the human behavior under the underbody blast scenario. To this end, Duke University and other academic institutions around the country have been task with characterizing the injurious response of the lumbar spine, amongst other body regions, under dynamic compression.

2.2 Materials and Methods

As different injury patterns are experienced by seated occupants depending on their initial posture (Spurrier et al., 2016), a nominal range of postures determined by the University of Michigan Transportation Research Institute (UMTRI) seated soldier study (Reed and Ebert, 2013) provided an appropriate characterization of injury potential for single or multilevel vertebral body fractures of the lumbar spine. Using these postures, dynamic compression tests were conducted on unembalmed human cadaveric thoracolumbar spines (T12-S1) at injurious loading conditions across three different specimen initial postures, which represented the nominal seated soldier posture ± a standard deviation. The cadaveric test protocol and battery was designed for two institutions: Duke University and the Medical College of Wisconsin (MCW). Testing was performed separately at both institutions in compliance with their respective Institutional Review Board experimental cadaver protocols and under the approval of the US Army.

Once the testing was completed, the data sets of both institutions were combined for use in developing an axial injury criterion.

2.2.1 Specimen preparation, testing and signal processing

Before testing, the structural integrity of each lumbar spine specimen was assessed through x-rays, CTs and microCT images generated at 100 μm x 100 μm x 100 μm resolution (Model XTH 225 ST, Nikon Metrology Inc., Brighton, MI, USA). Selected specimens had no evidence of joint degradation or osteophytes that could compromise their mechanical response. To avoid degradation, specimens were kept frozen at -20 °C and thawed at room temperature and normal humidity conditions 24 hours prior to preparation. This preparation procedure has been shown to have no significant effects on the mechanical properties of bones, ligaments, and the annulus fibrosus of the intervertebral discs (IVDs) (Galante, 1967; Sedlin and Hirsch, 1966; Tkaczuk, 1968). To avoid dehydration during tissue preparation and testing, specimens were maintained in saline-soaked gauze and were continuously hydrated with physiological saline. Preparation of the thoracolumbar spines included removal of ribs, musculature, fat, and periosteum without compromising the osteoligamentous structure and allowing for sensor placement as described in Ortiz-Paparoni et al. (2021) and Yoganandan et al. (2020).

Once specimens were dissected for sensor placement, they were fixated to the testing rig allowing motion only in the sagittal plane and they were aligned to match one of three postures estimating the real-world variance in seated position among military

occupants. These postures were denoted as nominal, pre-flexed, and pre-extended and were determined through the UMTRI seated solider study (Reed and Ebert, 2013). The pre-flexed and pre-extended postures represent one standard deviation from the mean nominal seated soldier posture (Figure 2-1). Specimens were then mounted to the testing rig to be subjected to dynamic compressive loading (Ortiz-Paparoni et al., 2021; Yoganandan et al., 2015a). Forces and moments at the proximal (T12) end of the thoracolumbar spine were recorded by a six-axis load cell (model MC5-6-5000, AMTI, Watertown, MA, USA) at the fixed crosshead of a custom servohydraulic Materials Testing Machine (MTS®, Eden Prairie, MN, USA) designed for Duke University. A six-axis load cell (model 3300J, Denton Inc., Troy, MI, USA) was used to record the thoracolumbar response at the T12 level for MCW's vertical accelerator testing device (Yoganandan et al., 2015a). Data was collected at 100 kHz and filtered with a 3000 Hz, phaseless 4-pole low-pass Butterworth filter to consider high frequency components. Using this filter, the allowable frequencies are higher than those outlined in SAE J211 CFC 1000 for automotive impact testing (SAE, 2007). Where appropriate, forces were compensated for inertial effects of the testing rig (Yoganandan et al., 2020b) and moments were translated from the load cell sensing element to the center of the T12-L1 IVD via rigid body translation.

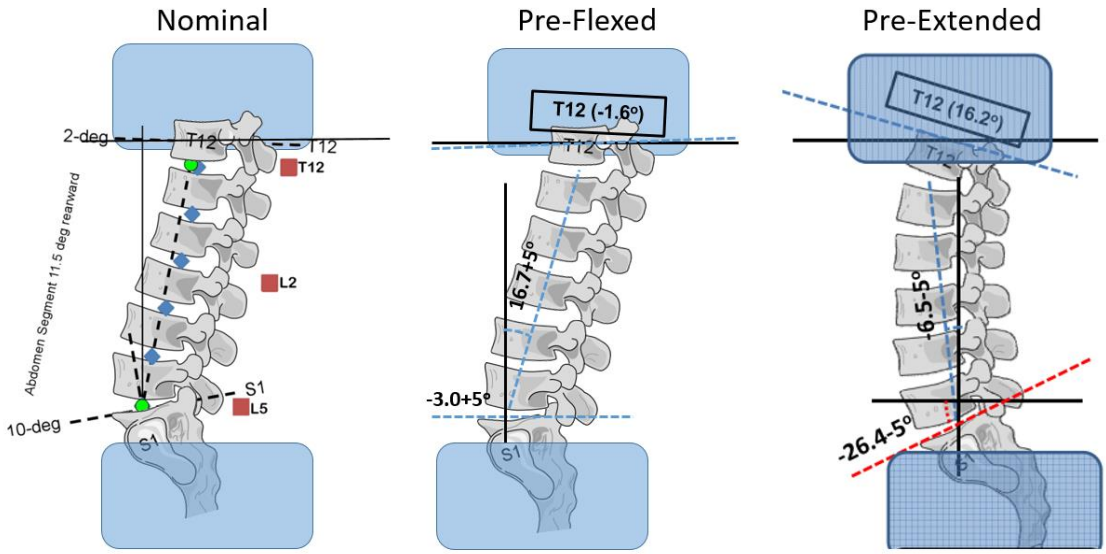

Figure 2-1. Lumbar spine posture derived from the Seated Soldier Study at UMTRI (Reed and Ebert, 2013). The representative range of one standard deviation from the mean nominal posture includes the nominal posture, the pre-flexed and pre-extended postures (Ortiz-Paparoni et al., 2021).

To aid in the determination of fracture, lumbar vertebral bodies (L1-L5) were instrumented with ten piezoelectric acoustic sensors for the Duke setup and four for the MCW setup (model S9225, Physical Acoustic Corporation, Princeton Junction, NJ, USA). To allow high-resolution timing of acoustic emissions with adequate bandwidth, acoustic sensors were sampled at 62.5 MHz at 14-bit resolution using a digital oscilloscope (model 5444B, Pico Technology, Tyler, TX, USA). To further aid identification of fracture onset, two to five strain gauges (model C2A-06-062LW-350, VPG Micro-Measurements, Raleigh, NC, USA) for the Duke setup and (model KFG-5-120-C1-11L1M2R, Omega Engineering, Stamford CT, USA) for the MCW setup were distributed across the L1 through L5 vertebral bodies. As with force and moment collection, strain gauges were sampled at 100

kHz and filtered with a 3000 Hz, phaseless 4th-pole low pass Butterworth filter to allow frequencies higher that those outlined in SAE J211. Figure 2-2 depicts the experimental setup and instrumentation used at Duke University.

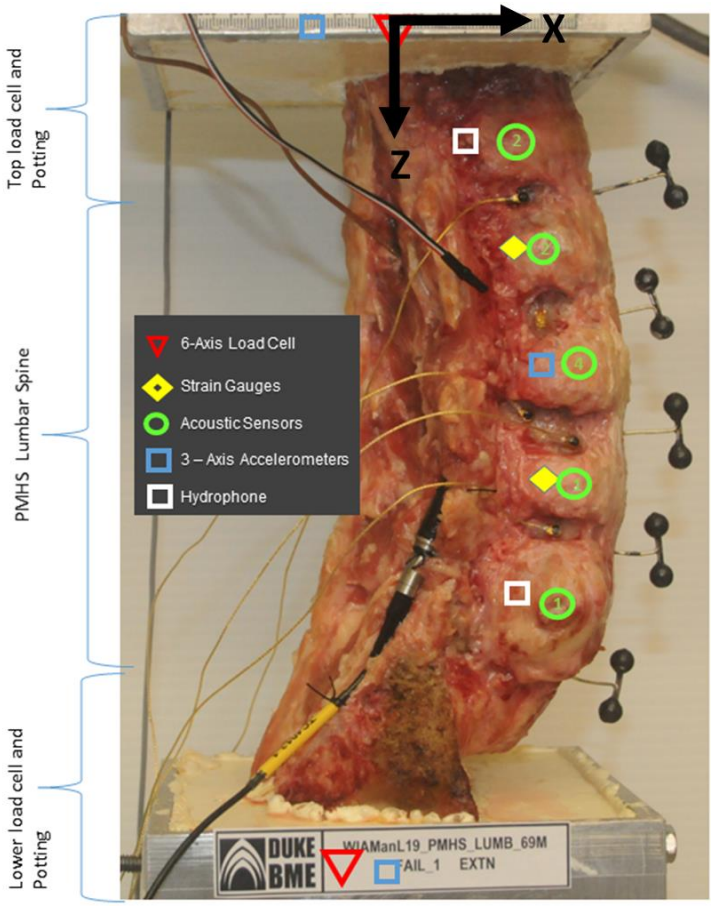

Figure 2-2: Duke experimental setup for a nominal extended specimen (LSPN19).

For Duke University's dynamic compression tests, once mounted in the MTS system, specimens were subjected to physiological preconditioning through 300 cycles of a 1 Hz oscillatory pulse at 1% engineering strain. Specimens were loaded from the distal end (S1) through the servohydraulic ram, in displacement control, with the proximal end

(T12) attached to the fixed end condition of the MTS crosshead. Displacement of the servohydraulic actuator was collected at 100 kHz by a linear variable displacement transducer (LVDT) (Measurement Specialties, Hampton, VA, USA), and filtered with a 3000 Hz, phaseless 4th-pole low pass Butterworth filter. Following preconditioning and prior to failure testing, specimens were subjected to two non-injurious dynamic compression conditions allowing 10 minutes for viscoelastic recovery between tests. Non-injurious input conditions were determined based on the outcomes of previous testing (Ortiz-Paparoni et al., 2020) and the repeatability of the specimen was assessed through the stiffness response (T12 axial force vs. S1 axial displacement). Once the non-injurious test battery was completed and repeatable behavior of the specimen was confirmed, the applied displacement was increased to a point where injury was predicted to occur (mean injury velocity of 4 m/s). Following the injury test, injuries were confirmed by visual examination, palpation and microCT images. Specific injury types, and vertebral body levels at which the injuries occurred, were assessed and documented during a necropsy procedure.

At the Medical College of Wisconsin, following bending preconditioning by manual manipulation, specimens were loaded inferiorly by the lever arm of a vertical accelerator device (Yoganandan et al., 2020b; Yoganandan et al., 2015a). The specimens were loaded at different velocities until injuries were detected or suspected (mean injury velocity of 6.5 m/s). The structural integrity of the specimen was assessed between tests

by palpation, lateral radiograph images, IVD height assessment, and joint laxity assessment by a clinician. Once the failure test was completed, the specimen was subjected to computed tomography and gross dissection to determine the injury outcome (Yoganandan et al., 2020b).

2.2.2 Injury Probability: Parametric Survival Analysis

Injury risk curves have been widely used in automotive biomechanics, for both civil and military applications, to inform human injury tolerance, advance occupant safety systems, and develop injury mitigation strategies (Arbogast and Maltese, 2015; Rupp, 2015; Salzar et al., 2015; Yoganandan et al., 2014; Yoganandan et al., 2016). These injury risk assessments can be derived from binary regression models (Kuppa et al., 2003; Seipel et al., 2001) or survival analysis (Cutcliffe et al., 2012; Kent and Funk, 2004; Yoganandan et al., 2020b). The latter allows to introduce different censoring status of the experimental outcomes to the analysis, providing more biomechanical information compared to sensor data alone.

Three parametric distributions were evaluated to determine the injury risk for the nominal ± standard deviation postures. The distribution with the best Anderson-Darling (AD) coefficient (which assesses whether a given sample is drawn from a given distribution and lower is better) (Anderson and Darling, 1954) was selected as the best representation of the injury risk. The equations that describe the three parametric distributions evaluated correspond to:

$$Lognormal: \frac{1}{2} + \frac{1}{2}\left(\mathrm{erf}\left(\frac{\ln(t) - \mu}{\sigma\sqrt{2}}\right)\right) \quad (2.1)$$

$$Loglogistic: \quad \frac{1}{1 + \left(\frac{t}{\sigma}\right)^{-\mu}} \quad (2.2)$$

$$Weibull: 1 - e^{-\left(\frac{t}{\sigma}\right)^{\mu}} \quad (2.3)$$

With the location (μ) and scale (σ) parameters estimated through maximum likelihood.

2.2.3 Injury Censoring

Timing of injuries during loading for the failure tests was assessed using acoustic sensors and strain gauges to provide interval censoring data for the injury metric analysis (Klein and Moeschberger, 2006). Without acoustic emission there is no presence of bony fracture, hence the lower bound of the censoring interval was determined through a combination of acoustic emissions and strain gauge responses for specimens that suffered single or multilevel vertebral body fractures. Acoustic emissions were filtered using a band pass filter with a phaseless Butterworth 4th order high pass 100 KHz and a Butterworth 4th order low pass filter at 1 MHz. Following this, signals were identified as 1.5x of the noise maximum with Morlet wavelet frequency identification. To supplement the acoustic data, large fractures were identified through abrupt decreases in strain response using strain gauges. Injury metric censoring for specimens that experienced vertebral body fractures was defined as the interval censored between the metric value (F_z) at initiation of fracture and its peak value during the failure test. For specimens that

had injuries different from vertebral body fractures, data was right censored with the peak value of the metric during the injury test. Survival analysis for determining the injury criteria was conducted using Minitab 19 (Minitab Inc., State College, PA, USA).

2.3 Results

The resulting combined dataset included 75 cadaveric thoracolumbar specimens, 64 of which resulted in a single or multilevel vertebral body fractures, 2 did not result in any injury and the remaining 9 resulted in other injury types (e.g., spinous process fractures). Figure 2-3 and Figure 2-4 depict some of the injuries incurred during dynamic compression at Duke University for the pre-flexed and pre-extended postures. A sample of the data set for injury outcome and posture is given in Table 2-1, the complete data set that includes all 75 tested specimens can be found in Table A.-1 of appendix A. The mean age, weight, stature, and body mass index (BMI) for the 75 male specimens were 66 ± 11 years, 81 ± 12 kg, 1.77 ± 0.05 m, 26 ± 4 kg/m^2 respectively.

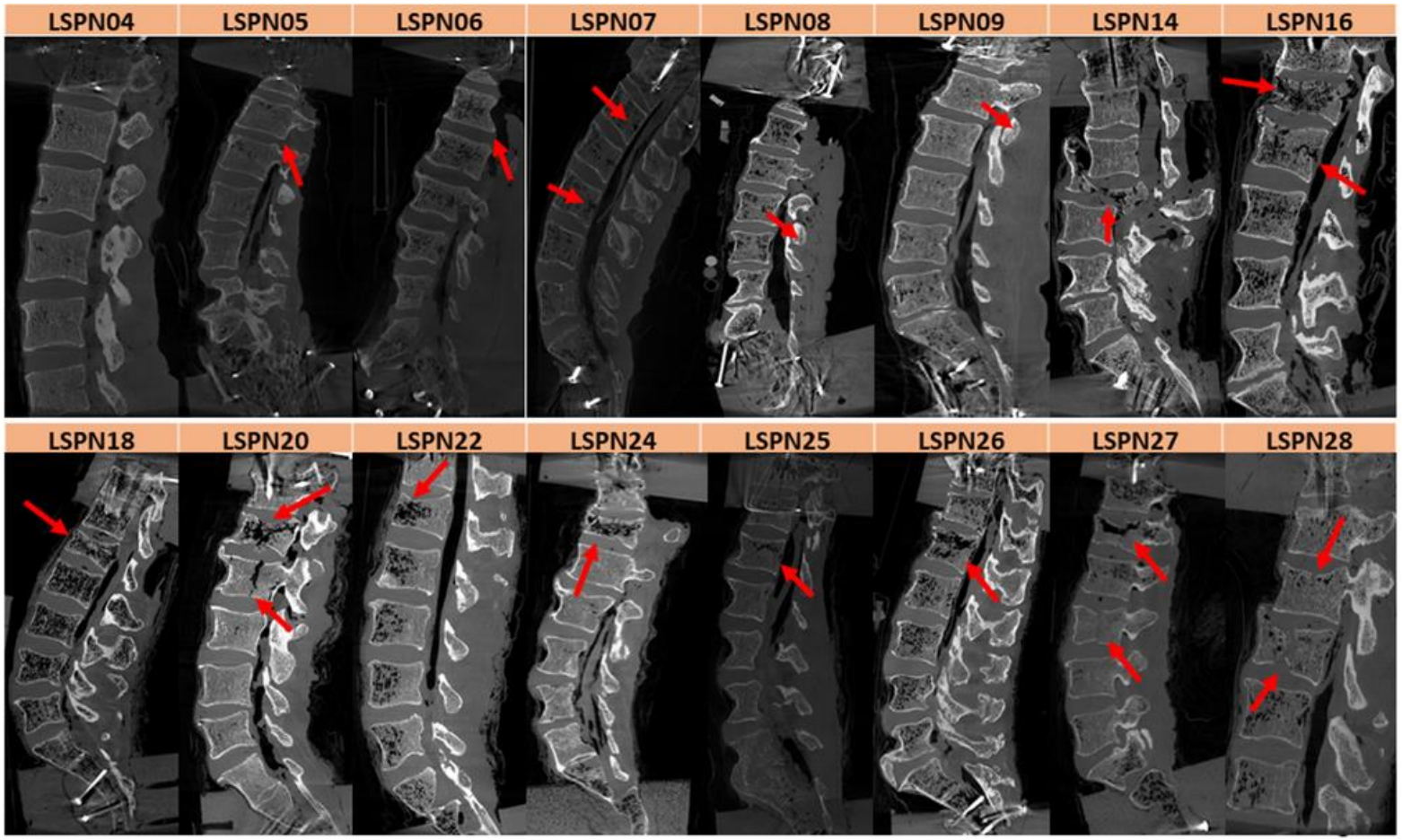

Figure 2-3: Sagittal microCT images depicting injuries carried out during pre-flexed testing.

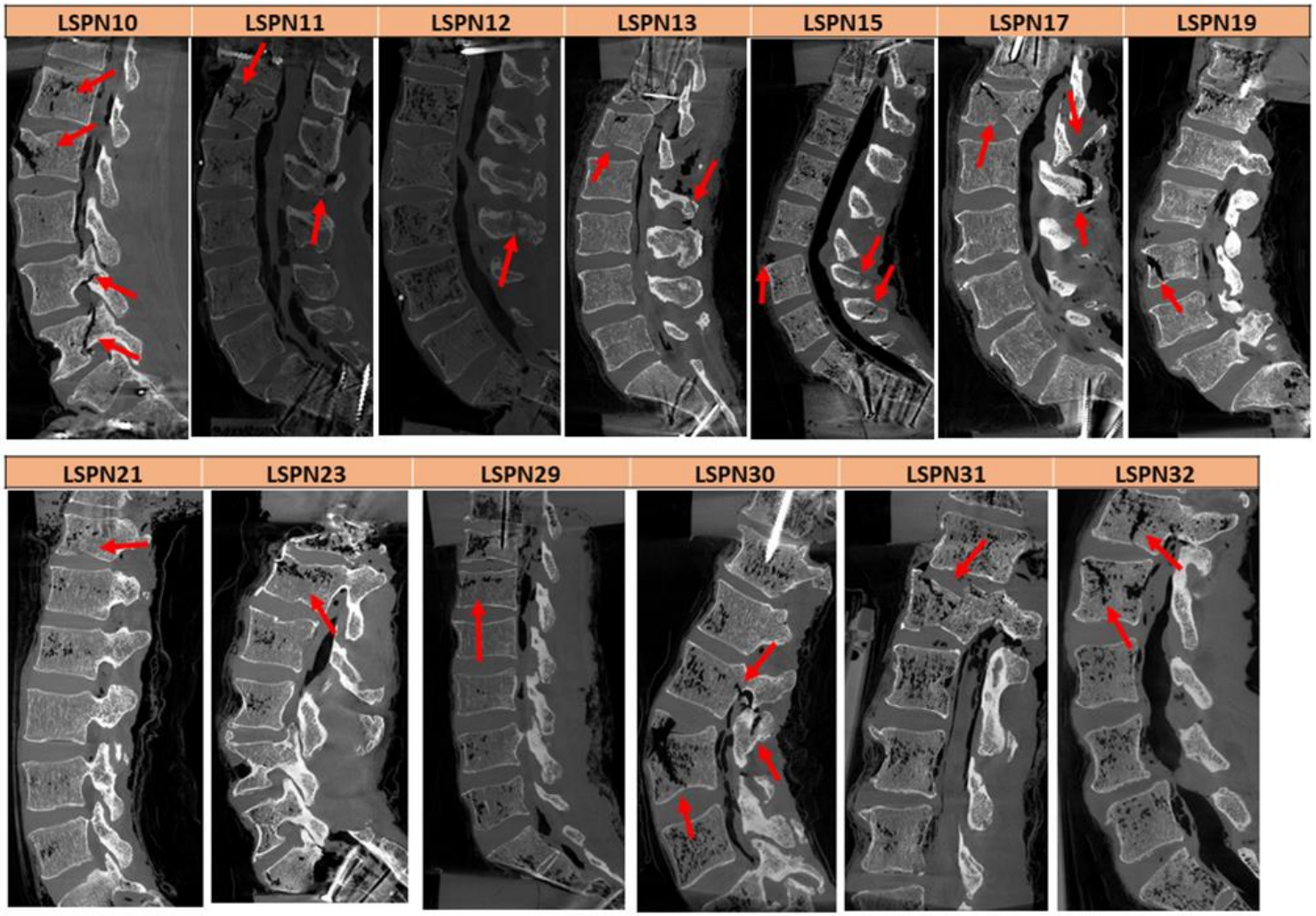

Figure 2-4: Sagittal microCT images depicting injuries carried out during pre-extended testing.

Table 2-1: Injury outcome for first 20 specimens of the test series. Posture definitions correspond to Nominal (N), Pre-Flexed (PF), and Pre-Extended (PE).

Test ID	Posture	Vert fx	Injury description
LSPN1	N	1	L1 vertebral body burst fx
LSPN2	N	1	L1 anterior vertebral body fx, L3 spinous process fx
LSPN3	N	1	L3 & L4 anterior vertebral body fx
LSPN4	PF	0	No injury
LSPN5	PF	0	L1 inf R facet fx; L1-L2 IVD ant rupture; L3-L4 IVD post rupture; L4-L5 IVD NP rupture
LSPN6	PF	0	L1 inferior left facet fx
LSPN7	PF	1	L1; L3 post crush fx; L3 L&R sup facet fx; L5 L sup facet fx; osteophyte fx L5 R inf facet; IVD rupture L2-L3 & L4-L5
LSPN8	PF	0	L3, L4 spinous process fx; L4 sup endplate fx
LSPN9	PF	0	L1 spinous process fx; L4, L5 endplate failures; T12-L1 IVD tear
LSPN10	PE	1	L1 anterior vertebral body fx, L1 bilateral transverse process fx; L1-L2 IVD NP rupture; L2 anterior vertebral body fx, L2 left superior articular process fracture, L2 ALL rupture; L3 spinous process fx; L3-L4 IVD failure; L4 bilateral pedicle fx; L5 bilateral pedicle fx
LSPN11	PE	1	L1 vertebral body burst fx, L1 bilateral pedicle fx, L1 inferior left capsular ligament rupture; L2 superior right facet fx, L2 spinous process fx; L4 spinous process fx, L4 bilateral pedicle fx; L5 superior left articular process fx, L5 left pedicle fx
LSPN12	PE	0	L2 superior endplate fx; L3 spinous process fx, L3 minor superior endplate fx; S1 vertebral body fx, bilateral fx of sacrum ala
LSPN13	PE	1	L1 vertebral body fx, L1 bilateral pedicle fx; L2 spinous process fx
LSPN14	PF	1	L2 vertebral body burst
LSPN15	PE	0	L3-L4 disc disruption; L4 spinous process fx; L5 spinous process fx; S1 vertebral body fx
LSPN16	PF	1	L1, L2 vertebral body crush
LSPN17	PE	1	L1 vertebral body burst fx, L1 bilateral pedicle fx, L1 spinous process fx; L2 spinous process fx
LSPN18	PF	1	L1 Vertebral body burst
LSPN19	PE	1	L3 anterior vertebral body fx, L3 spinous process fx
LSPN20	PF	1	T12 vertebral body fx; L1 vertebral body crush; L1 bilateral lamina fx; L2 vertebral body crush

Values of 1 for the "Vert fx" column correspond to the presence of either a single or a multilevel vertebral body fracture. Values of 0 correspond to the presence of a different injury type or absence of injury.

2.3.1 Injury Censoring

For a single failure test, censoring used sensor data to identify the lower and upper censoring bounds. Acoustic emission results were supplemented by identifying major changes in the response of the strain gauges to corroborate failure. The acoustic sensors are more sensitive than the strain gauge to low level bony fractures, therefore the acoustic sensors showed evidence of bone fracture earlier or at the same time than the strain gauge (Figure 2-5).

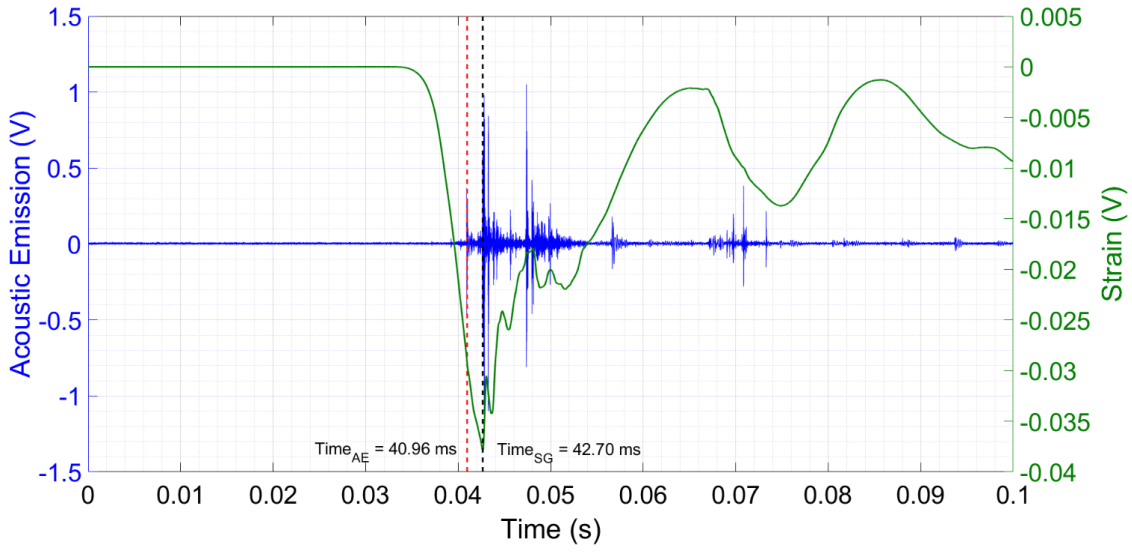

Figure 2-5: Example of fracture initiation determination for lower bound of censoring interval for Duke test LSPN31. Blue trace corresponds to band pass filtered (100 KHz – 1000 KHz) acoustic emission of L2 sensor. Green trace represents L2 strain gauge measurement. Initiation of acoustic emission (red dashed line) indicated by acoustic signal above a 0.25V threshold at 40.96 ms. Strain gauge fracture indication (dashed black line) coincides with acoustic emission threshold of ~ 1V at 42.7 ms (Ortiz-Paparoni et al., 2021).

The earliest times are used for data censoring. In some cases, the noise floor prevented the use of acoustic signals for fracture identification. However, where available,

the acoustic sensors are consistent with the fracture assessment, and the strain gauge data was available for fracture identification for the remainder of the tests. Representative metric values (F_z, F_x, F_r, M_y) for the initiation of fracture and at maximum axial force are given in Table 2-2. This information for all 75 tested specimens can be found in Table A-2 of appendix A.

Table 2-2: Injury metric values at the T12-L1 IVD center for first 20 specimens of test series. Note that the upper and lower bounds of the interval censored data are defined by the value at peak force and the value at the fracture initiation respectively. Specimens that did not present vertebral body fractures were designated as right censored.

Test ID	Value at Peak Axial Force			Fracture Initiation (Acoustic + Strain Gauge Onset)			Vert fx
	F_z (N)	M_y (Nm)	F_x (N)	F_z (N)	M_y (Nm)	F_x (N)	
LSPN1	2474	14	681	704	10	54	1
LSPN2	6447	75	286	6066	28	560	1
LSPN3	7945	33	1157	1754	7	87	1
LSPN4	5692	134	-78	-	-	-	0
LSPN5	4302	99	70	-	-	-	0
LSPN6	5854	44	-1339	-	-	-	0
LSPN7	3635	67	-1118	2464	1	583	1
LSPN8	4766	57	-525	-	-	-	0
LSPN9	7516	52	-684	-	-	-	0
LSPN10	7677	28	196	1621	30	17	1
LSPN11	5872	69	-715	4272	273	43	1
LSPN12	4005	15	1383	-	-	-	0
LSPN13	5753	104	511	1053	118	93	1
LSPN14	6633	242	62	2482	34	162	1
LSPN15	5211	29	-253	-	-	-	0
LSPN16	7442	4	-2411	2089	5	1245	1
LSPN17	5089	55	697	1091	101	123	1
LSPN18	7680	124	106	2070	23	727	1
LSPN19	6585	68	436	661	108	173	1
LSPN20	7316	35	-1840	1543	69	946	1

2.3.2 Injury Probability

The three tested distributions had similar Anderson-Darling coefficients, with the loglogistic distribution resulting in the lowest AD coefficient across all tested postures (Table 2-3). Hence, the loglogistic distribution was chosen to represent the injury risk for all three tested postures (Figure 2-6)

Table 2-3: Anderson-Darling coefficients for three assessed distributions. Note that the loglogistic distribution has the lowest AD across the tested postures.

	Anderson-Darling Coefficient		
Posture	**Lognormal**	**Loglogistic**	**Weibull**
Nominal	1.24	0.792	1.141
Nominal Flexed	0.771	0.749	0.838
Nominal Extended	0.856	0.831	0.945

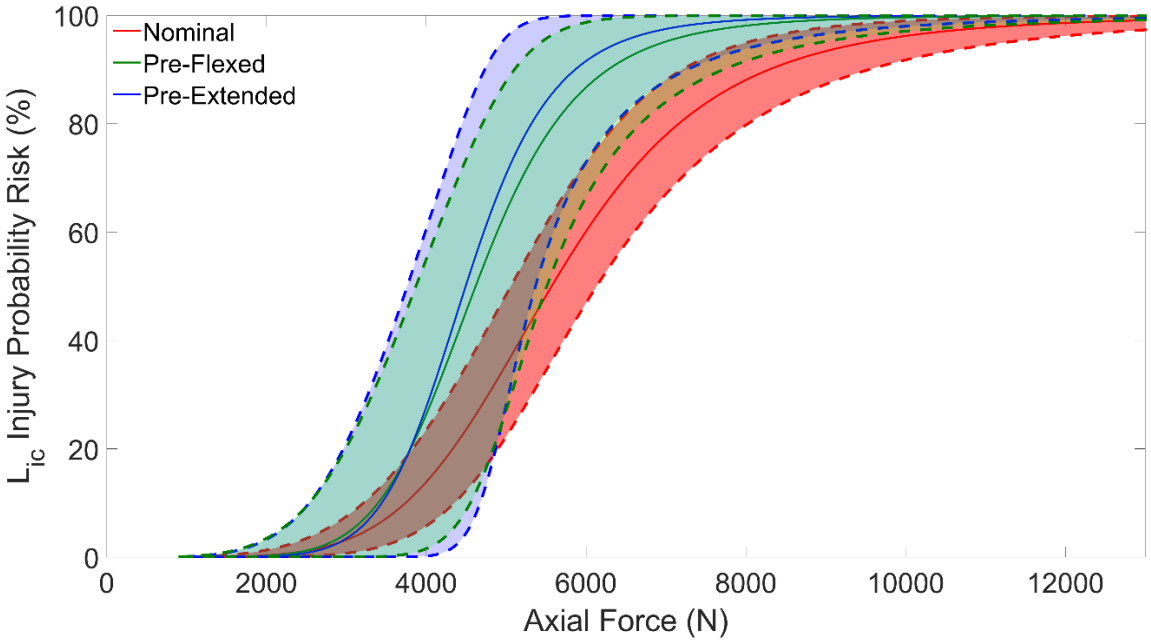

Figure 2-6: Human Injury Probability Curve (HIPC) for three postures under dynamic compression. Corridors show a censored survival analysis with a loglogistic regression for nominal posture (red, n = 46), pre-flexed posture (green, n = 16), and pre-extended posture (blue, n = 13).

Across the three tested postures the nominal posture presented a higher injury tolerance to the axial force, with the 50% injury risk happening at 5569 N (Table 2-4).

Table 2-4: Selected injury risk values of axial force (F_z) for lumbar specimens subjected to dynamic compression in the nominal posture.

Risk Level	F_z (N)	Lower 95% CI	Upper 95% CI	NCIS
0.05	3265	2722	3917	0.37
0.1	3739	3213	4351	0.30
0.2	4331	3830	4898	0.25
0.3	4776	4286	5321	0.22
0.4	5174	4682	5718	0.20
0.5	5569	5057	6132	0.19
0.6	5994	5440	6604	0.19
0.7	6494	5863	7193	0.20
0.8	7160	6387	8027	0.23
0.9	8294	7207	9546	0.28
0.95	9498	8015	11255	0.34

The pre-flexed (Table 2-5) and pre-extended (Table 2-6) postures had similar injury tolerance, with the 50% risk being 4618 N and 4493 N respectively.

Table 2-5: Selected injury risk values of axial force (F_z) for lumbar specimens subjected to dynamic compression in the pre-flexed posture.

Risk Level	F_z (N)	Lower 95% CI	Upper 95% CI	NCIS
0.05	3060	2166	4322	0.70
0.1	3397	2535	4551	0.59
0.2	3804	2991	4839	0.49
0.3	4102	3323	5063	0.42
0.4	4363	3607	5278	0.38
0.5	4618	3871	5509	0.35
0.6	4887	4130	5783	0.34
0.7	5198	4400	6142	0.34
0.8	5605	4703	6681	0.35
0.9	6278	5104	7721	0.42
0.95	6969	5434	8937	0.50

Table 2-6: Selected injury risk values of axial force (F_z) for lumbar specimens subjected to dynamic compression in the pre-extended posture.

Risk Level	F_z (N)	Lower 95% CI	Upper 95% CI	NCIS
0.05	3143	2185	4522	0.74
0.1	3442	2534	4674	0.62
0.2	3798	2962	4870	0.50
0.3	4054	3268	5029	0.43
0.4	4278	3527	5188	0.39
0.5	4493	3762	5367	0.36
0.6	4720	3987	5588	0.34
0.7	4980	4211	5889	0.34
0.8	5316	4448	6354	0.36
0.9	5866	4733	7271	0.43
0.95	6423	4944	8344	0.53

The normalized confidence interval size (NCIS), given by equation 2.4, was consistently lower across the injury risk for the nominal posture when compared to the

pre-flexed and pre-extended postures. The NCIS for the pre-flexed and pre-extended postures was similar across all the injury risk values, with the pre-flexed posture presenting slightly better values (Figure 2-7).

$$NCIS = \frac{UB_p - LB_p}{M_p} \tag{2.4}$$

In equation 2.4 UB_P is the upper 95% confidence interval (CI) of the injury probability curve, LB_P is the lower 95% CI and M_P is the mean metric value.

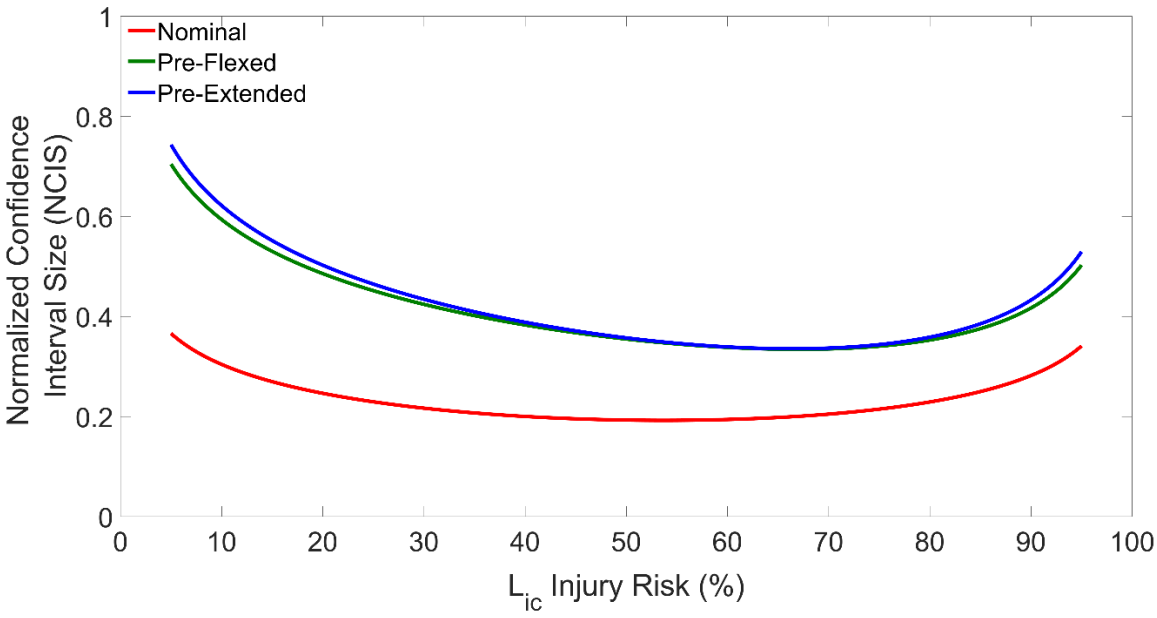

Figure 2-7: Normalized Confidence Interval Size (NCIS) for the axial loading metrtic for three tested postures: nominal (n = 43), pre-flexed (n = 16), pre-extended (n = 13).

2.4 Discussion

This chapter elucidates the axial force injury tolerance of the lumbar spine when subjected to UBB scenarios. Further it expands the current literature on lumbar spine axial tolerance (Duma et al., 2006; Yoganandan et al., 2020a; Yoganandan et al., 2020b) by introducing the risk analysis for two lumbar spine postures that represent the standard deviation from the nominal seated soldier posture.

A key contribution of this study is the use of interval censoring, which is crucial in producing improved confidence intervals in survival analysis owing to the use of additional biomechanical information over right censored, left censored, and exact data alone. One strategy to determine interval censoring data for biomechanical structures consists of taking the maximum metric value obtained from a non-failure test as the lower bound of the censoring interval and taking the highest metric value obtained during a failure test as the upper bound of the censoring interval. Exact data is sometimes used by defining the failure point as the maximum metric value obtained during a failure test. While these strategies provide valuable biomechanical information to the injury risk model, they are limited in bounding the cadaver failure point since the fracture of interest in a complex system, such as the lumbar spine, does not necessarily occur at the maximum metric value. Non-failure tests may stay considerably below injury thresholds. Using the acoustic emission techniques and strain response we can determine the onset of the spine injury during a failure test, hence reducing the uncertainty of the lower bound of the

censoring interval. With this strategy the lower bound of the censoring interval is closer to the initiation of the failure event (Figure 2-5) and the upper bound remains as the maximum metric value of the failure test. This approximation of the censoring interval represents an improvement over standard censoring techniques by narrowing the occurrence of fracture within the metric of interest, resulting in improved confidence intervals for the injury metric.

The 50% risk of fracture for lumbar spines in the nominal posture (Table 2-4) of 5569 N is in agreement with results reported by Yoganandan et. al, (2020) with the MCW data alone, and represented the highest axial force tolerance of the three postures evaluated. The pre-extended and pre-flexed postures had very similar injury risk assessments (Figure 2-6) with the pre-extended posture presenting an 50% injury risk at 4493 N (Table 2-6) and the pre-flexed posture having 4618 N tolerance at 50% injury risk (Table 2-5). Further, the nominal posture analysis resulted in the lowest NCIS values when compared to the other two postures (Figure 2-7), which is to be expected since the total number of specimens evaluated for this posture was approximately 3 times higher than the other two postures (43 for nominal vs. 16 for pre-flexed and 13 for pre-extended). However, NCIS values are expected to decrease if more specimens were added to the pre-flexed and pre-extended postures.

From the perspective of beam theory, differences in the injury tolerance across postures could be explained by increased moment contribution to failure in the more

flexed and extended postures. Since the moment is not included in the axial compression injury assessment, the effect of moment would be to reduce the apparent axial tolerance in off-nominal conditions. Contributing to base beam theory effects, the off-nominal postures may change the center of moment action of the complex system which can introduce moments that are making a higher contribution to the injury event in the off-nominal postures. This suggests that a single axial force metric alone does not capture the full potential of the injury risk, making the case for the development of an injury criteria that considers the contributions of the bending moment to the injury risk.

An additional explanation may be the reduction of the spine range of motion incurred by the loss of lordosis of the pre-flexed and pre-extended postures. This could result in different anatomical interactions that happen at higher displacements and forces in the compressive event for the nominal posture. This is similar in concept to the simple beam theory approach. Another contributor could be the addition of preloads into the system when subjecting the spine to the of-nominal posture conditions. However, spines were allowed to undergo viscoelastic recovery before testing, and pre-load values were closely monitored during the potting procedures to ensure no significant strain was added to the system.

It should be noted that the values reported in this chapter for the axial force injury tolerance of the lumbar spine are strictly applicable to the narrow range of nominal and off-nominal seated soldier postures identified in Figure 2-1. Thus, these injury risk

assessments should not be applied beyond the established range of postures or interchanged between them. Additionally, the dynamic compression tests conducted in this study ranged on loading rates applicable to UBB scenarios, therefore this injury criteria should not be applied for compressive events below 1 m/s initial loading velocity. Further, the human cadavers used for this study may have presented disc degeneration in accordance with their age, hence caution should be exercised when applying the L_{ic} to younger and healthier populations. Finally, it should be recognized that this injury criteria applies to single or multi-body vertebral body fractures, and further work needs to be done to address different injury outcomes such as posterior element fractures, and soft tissue injuries.

3 The Combined Loading Injury Criterion

In this chapter, the influence of the bending moment on the injury tolerance of the lumbar spine was evaluated using a combined metric that considers both the axial force and bending moment of the loading event. A combined loading lumbar spine vertebral body fracture injury criterion (CL_{ic}) across a range of postures was established from the 75 cadaveric lumbar spines tests described in chapter 2.[1]

3.1 Introduction

Vertical loading significantly contributes to the overall loading of the spine during underbody blast events. (Vasquez et al., 2018; Yoganandan et al., 2013; Yoganandan et al., 2020b). Axial force injury criterion such as the one presented in chapter 2 or that developed by Yoganandan et al. (2020) can aid in developing biofidelic surrogates, establishing finite element models, understanding injury, and can ultimately contribute to injury mitigation strategies. However, these studies do not account for the bending response of the thoracolumbar spine. Given the complex geometry and loading path during UBB, the position of the spine will not necessarily be in line with the loading in the instant that the underbody force reaches the pelvis. Therefore, the loading pattern

[1] This chapter contains materials originally published in Annals of Biomedical Engineering: 49, 3018-3030 (2021). (DOI: https://doi.org/10.1007/s10439-021-02823-x) © 2022 Springer Nature Switzerland AG. Part of Springer Nature. This reuse is permitted under the publisher's copyright terms. Collaborators on this work are gratefully acknowledged. (Ortiz-Paparoni et al. 2021)

exhibited during the dynamic compression events is not captured by force data alone. Current literature has yet to broadly consider the effect of moment on the overall loading of the spine in UBB. While vertical loading injury criteria represent an important advancement in understanding lumbar spine injuries during UBB events, considering only vertical loading can underestimate the influence of moment loading on injury outcome. Therefore, a combined injury criterion considering both sagittal forces and bending moment can lead to an expanded assessment of injury risk that can ultimately lead to future vehicle designs or mitigation strategies to reduce the incidence of these injuries.

3.2 Materials and Methods

The human cadaveric lumbar spines used for the development of the combined injury criterion are the same as those used for the development of the axial loading injury criterion. Therefore, the experimental methodology followed for this specific aim can be reviewed in section 2.2 of chapter 2.

However, to develop the combined injury metric further considerations were performed for the analysis.

3.2.1 Moment decorrelation

To provide a consistent basis for comparison across tests, collected load cell data was translated to anatomical reference locations via rigid body transformations, with the

bending moment translation given by equation 3.1. For the combined loading injury criteria, the use of an effective moment center at T12-L1 was necessary to avoid spurious bending moments that are correlated with the axial force (F_z) but do not provide additional stress from bending on the anterior or posterior surface of the functional spinal unit. Errors in assessing the actual biomechanical moment center increases the correlation between the axial force component and the bending moment (M_y) component, adding uncertainty to the determination of a combined injury criteria. To reduce this uncertainty and account for the independent effects of M_y and F_z in the combined lumbar injury criteria (CL_{ic}), the moment arm of the bending moment was optimized to minimize the Pearson correlation coefficient between the bending moment (M_y) and the axial force (F_z) at T12 (Figure 3-1).

$$My_{Translated} = My_{Measured} + F_z * moment\ arm \tag{3.1}$$

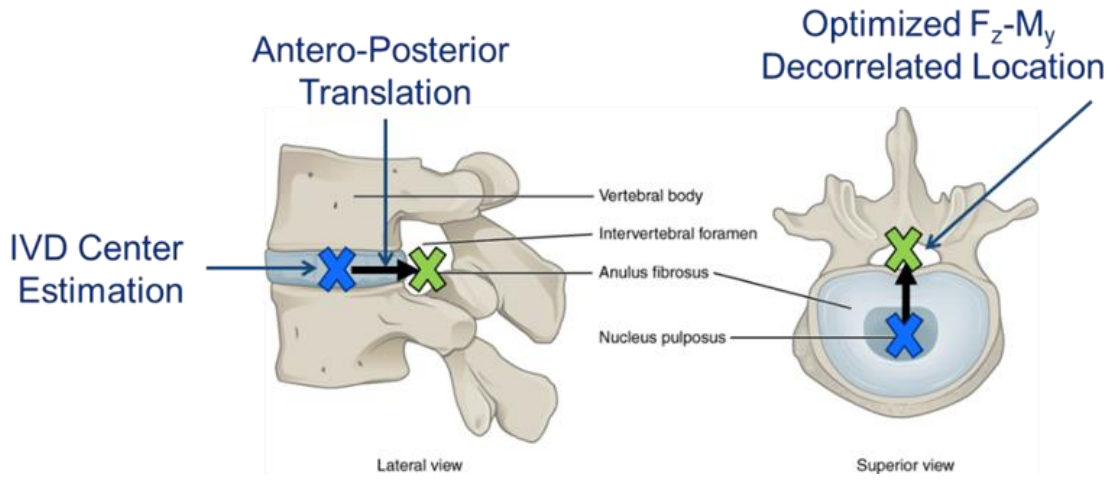

Figure 3-1: Optimized moment arm (antero-posterior translation) of F_z-M_y decorrelated moment based on reduction of Pearson correlation coefficient between M_y and F_z during loading to first major failure (Ortiz-Paparoni et al., 2021).

3.2.2 Lumbar Injury Criteria: combined loading

Similar to section 2.2.2 of chapter 2, three distribution functions (Weibull, Loglogistic, and Lognormal) were evaluated for the development of a combined loading (CL_{ic}) injury risk. A combined loading injury metric criteria of the peak sagittal resultant force (F_r) at the T12-L1 moment center and bending moment at T12-L1 (M_y) was used to incorporate the contributions of both the bending moment and force(s) to the injury outcome in all postures. This allowed combination and inclusion of the entire Duke and MCW lumbar data sets. The combined loading injury metric was based on prismatic beam failure analysis, similar to that used by the US Department of Transportation for assessment of the Hybrid III ATD neck in crash testing (Eppinger et al., 1998). This formulation, derived for nonlinear prismatic beams (Figure 3-2), incorporates force and moment as:

$$\kappa = \frac{F_r}{F_{r,\,crit}} + \frac{M_y}{M_{y,crit}}. \tag{3.2}$$

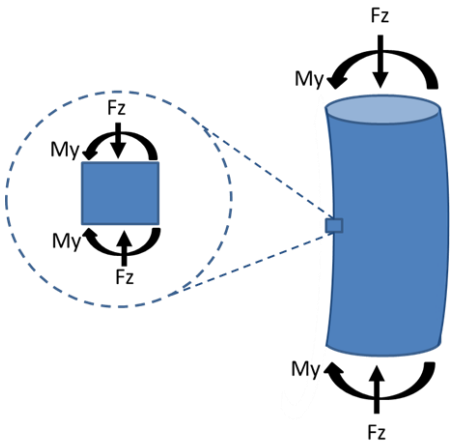

$$I = \frac{\sigma_{F_z}}{\sigma_{F_{z,crit}}} + \frac{\sigma_{M_y}}{\sigma_{M_{y,crit}}}$$

$$I = \frac{F_z}{F_{z,crit}} + \frac{M_y}{M_{y,crit}}$$

Figure 3-2: Combined loading stress and force failure criteria based on prismatic beam formulation.

The combined metric κ was calculated by determining the $F_{r,crit}$ and $M_{y,crit}$ values through a minimization of the normalized confidence interval defined by equation 2.4 (Arun et al., 2014; Bass et al., 2010).

To minimize the NCIS an initial value of $F_{r,crit}$ and $M_{y,crit}$ were assumed and a κ metric was calculated for the failure tests at the maximum values of the metrics. Subsequently, the κ metric was calculated with known non-failure points based on acoustic emission and strain response sensor evidence of non-failure. With the previously calculated κ values, a risk function CL_{ic} (through the aforementioned distribution functions) and the NCIS were determined. Posteriorly $F_{r,crit}$ and $M_{y,crit}$ were changed based on a line search algorithm (Wolfe, 1969) and the process was repeated until the calculated κ metric minimized the NCIS across risk levels from 1% through 99%.

3.3 Results

As described in chapter 2 the combined dataset included 75 cadaveric specimens, 64 resulted in a single or multilevel vertebral body fractures, 2 did not result in any injury and the remaining 9 resulted in other injury types. The mean age, weight, stature, and BMI for the 75 male specimens were 66 ± 11 years, 81 ± 12 kg, 1.77 ± 0.05 m, 26 ± 4 kg/m^2 respectively.

3.3.1 Moment decorrelation

A large correlation between the axial force (F_z) and the bending moment (M_y) was observed, with a mean value of 80% ± 26% across the 75 tested specimens (Figure 3-3). New antero-posterior translations that minimized the correlation across F_z and M_y were determined with a median and standard error values of 0.92 ± 0.2 cm from the estimated center of the IVD (Figure 3-4). It is important to note that this translation only affects the M_y values, F_z and antero-posterior force values (F_x) are invariant to this translation.

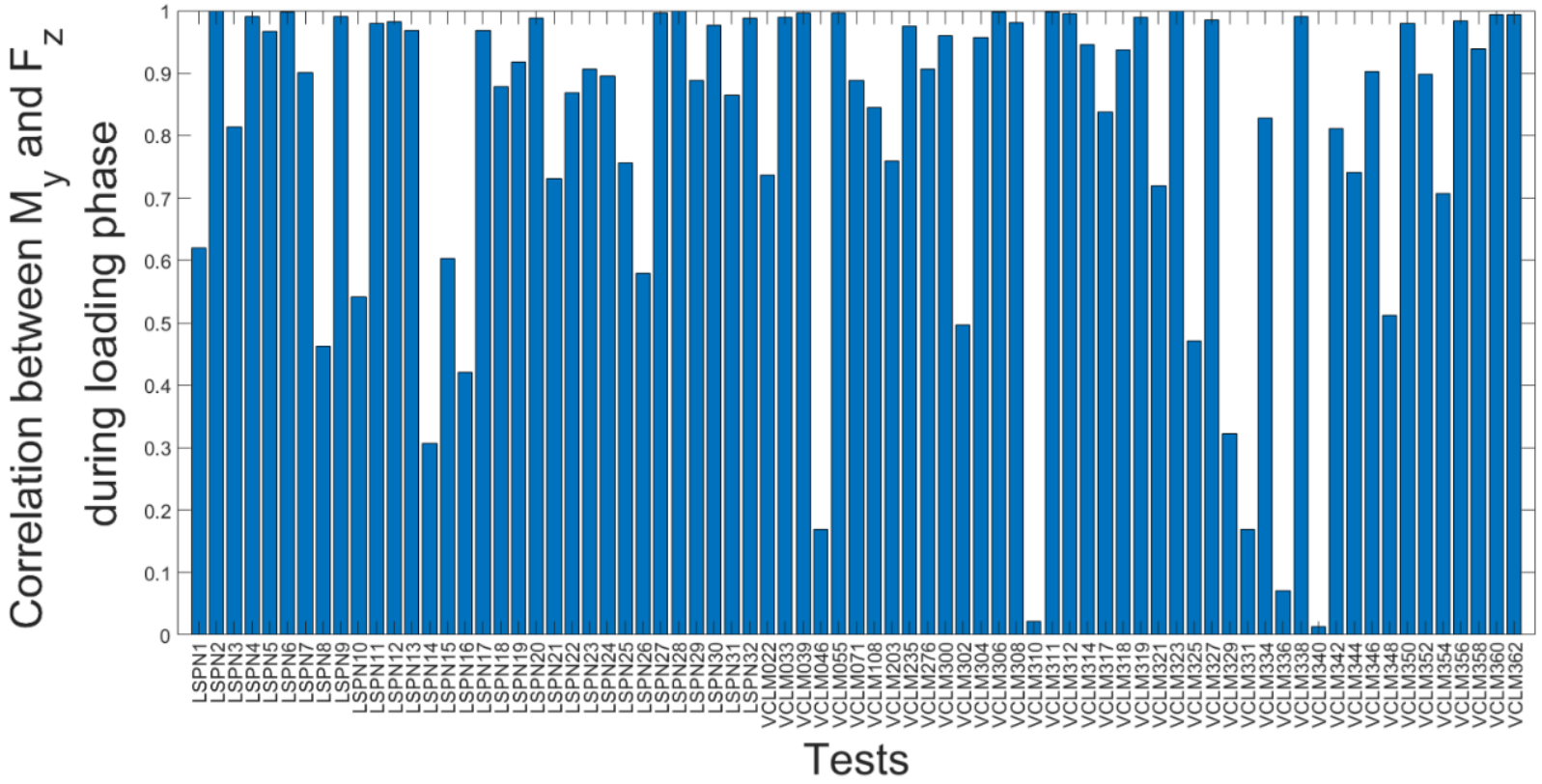

Figure 3-3: Correlation of F_z and M_y for Duke and MCW lumbar tests. The majority of the tests show highly correlated data owing to differences between the effective moment center of the loading event and the estimated geometrical center of the T12-L1 intervertebral disc (Ortiz-Paparoni et al., 2021).

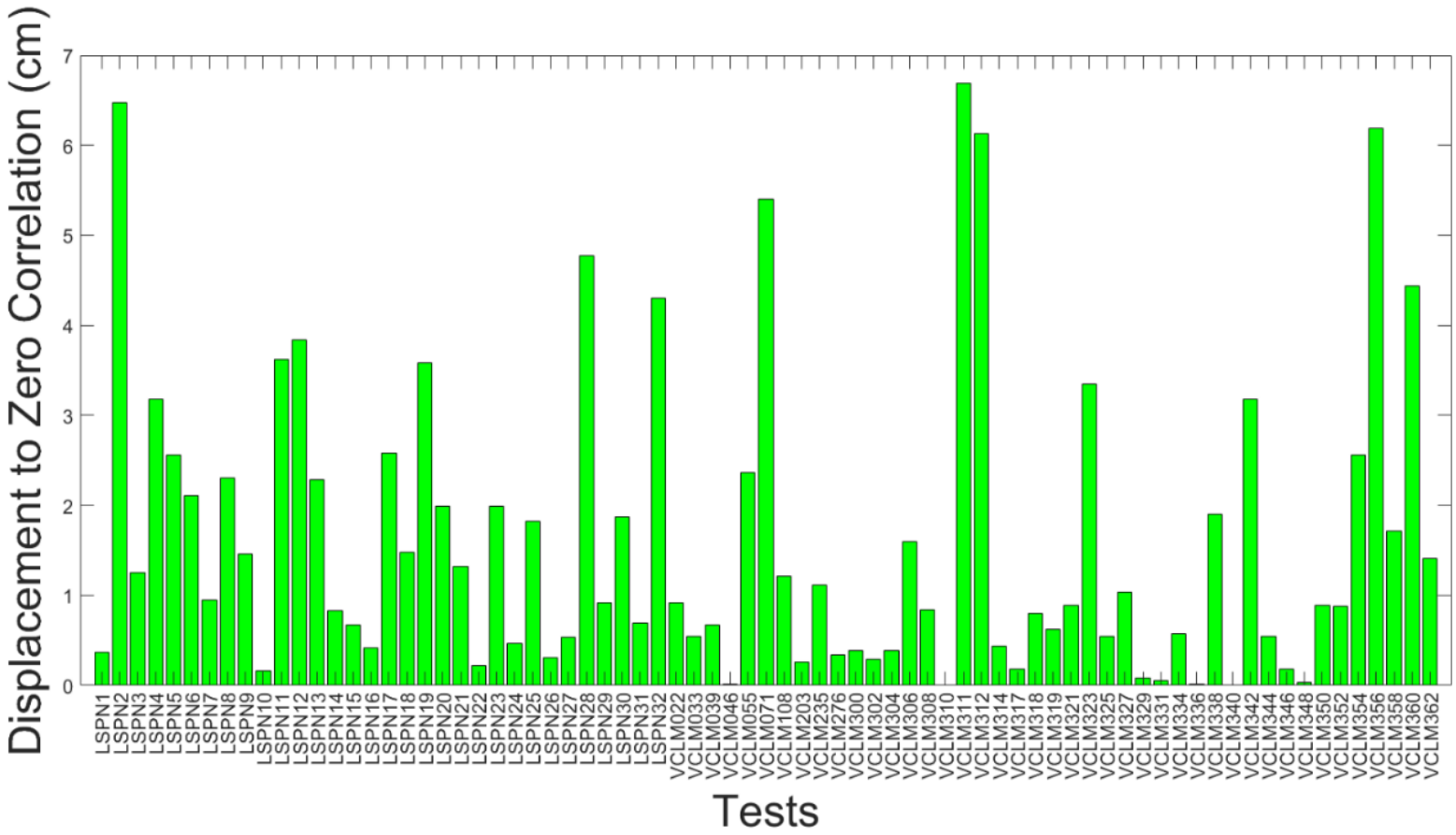

Figure 3-4: Posterior translations of the estimated effective moment arm location that minimizes the correlation between F_z and M_y for Duke and MCW thoracolumbar data set (Ortiz-Paparoni et al., 2021).

3.3.2 Combined loading injury criterion (CL_{ic})

All three distributions had similar Anderson-Darling coefficients (Table 3-1). Furthermore, they had similar values with the lognormal formulation improving confidence intervals for risk values below 20% and above 80%. Hence, a lognormal distribution was selected as the optimal representation for the investigation of the injury risk curves (IRCs). The resultant sagittal force at the T12-L1 joint was mostly dominated by the axial component with the (Fr – |Fz|)/Fr ratio below 5%. Therefore, combined loading and axial injury curves were calculated using the resultant sagittal force. The mean injury probability along with the lower and upper bound of the 95% confidence interval for the proposed combined metric and an axial force injury metric are presented in figure 6.

Table 3-1 Anderson-Darling (AD) coefficient for each distribution parametric distribution.

Metric	Distribution	AD
$CL_{ic}(\kappa)$	Weibull	1.47
$CL_{ic}(\kappa)$	Loglogistic	0.82
$CL_{ic}(\kappa)$	Lognormal	1.05

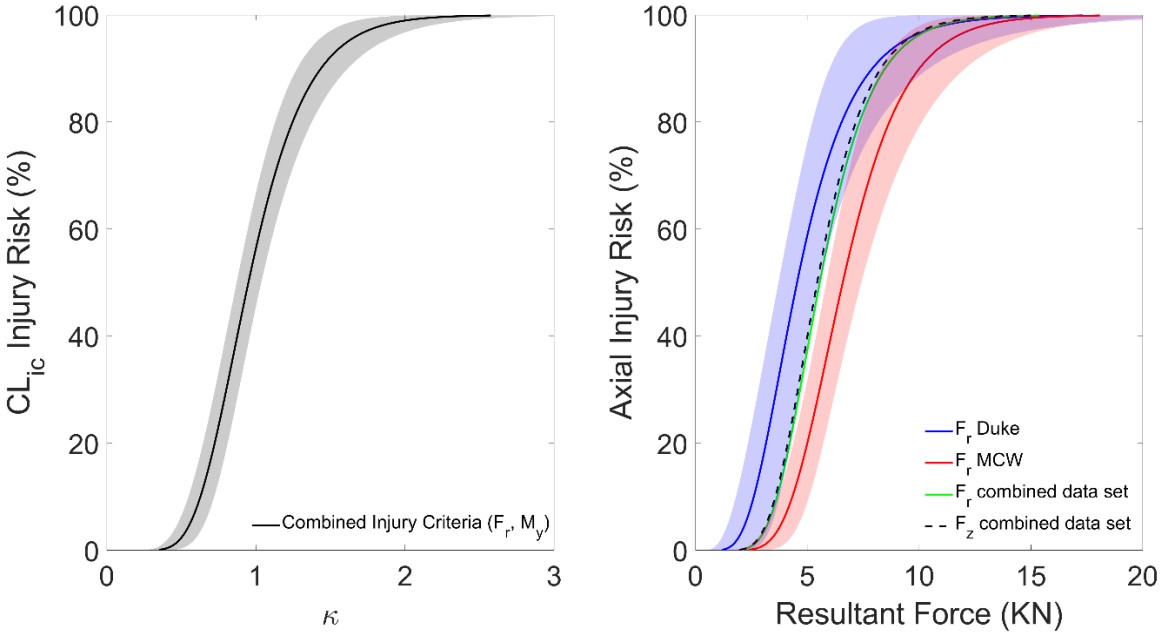

Figure 3-5: Injury risk comparison of the lumbar spine during dynamic compression. Left: Lumbar Injury Criteria (CL_{ic}) for the integrated Duke and MCW data set using a combined loading metric that incorporates the resultant sagittal force and decorrelated bending moment at the T12-L1 joint. Right: Force injury risk curves, note that axial force (dashed black line) and resultant sagittal force (green) for the integrated data set are highly similar. Furthermore, the Duke and MCW data sets present a 50% risk of injury at 4.54 KN and 6.59 KN for n = 32, and n = 43 respectively.

The resulting lumbar injury criteria (CL_{ic}) with the combined metric (κ) using the T12-L1 resultant compressive force (F_r) and the decorrelated bending moment (M_y) is given by the location (γ) and scale (λ) parameters of the Lognormal cumulative density function, which were determined to be -0.0578 and 0.3214, respectively (Equation 3.3). The critical parameters of equation 3.2 were optimized to $F_{r,crit}$ = 5824 N and $M_{y,crit}$ = 1155 Nm (Equation 3.4).

$$L_{ic}(\kappa; -0.0578, 0.3214) = \frac{1}{2} + \frac{1}{2} \cdot \mathrm{erf}\left(\frac{\ln(\kappa) - 0.0578}{0.3214 * \sqrt{2}}\right) \tag{3.3}$$

$$\kappa = \frac{F_r}{5824} + \frac{M_y}{1155} \tag{3.4}$$

The NCIS was determined across the combined loading metric of the integrated Duke and MCW data set, and the independent resultant sagittal force-based IRCs for Duke and MCW (Figure 3-6). A combined metric (κ) of 1 at the T12-L1 joint corresponds to a 50% probability of lumbar spine vertebral body fracture. The injury risk decreases with decreasing combined metric value with 0.84, 0.66, and 0.59 corresponding to a 30%, 10%, and 5% chance of vertebral body injury, respectively (Table 3-2).

Table 3-2: Selected CL_{ic} values for the T12-L1 Resultant Force (Fr) and Bending Moment (My) Combination Metric (Ortiz-Paparoni et al., 2021).

Risk Level	κ	Lower 95% CI	Upper 95% CI	NCIS
0.05	0.59	0.50	0.69	0.32
0.1	0.66	0.58	0.76	0.27
0.2	0.76	0.68	0.85	0.23
0.3	0.84	0.76	0.93	0.20
0.4	0.92	0.84	0.99	0.19
0.5	1	0.91	1.09	0.17
0.6	1.08	1	1.07	0.17
0.7	1.18	1.08	1.29	0.18
0.8	1.31	1.19	1.44	0.20
0.9	1.51	1.34	1.70	0.23
0.95	1.70	1.48	1.94	0.27

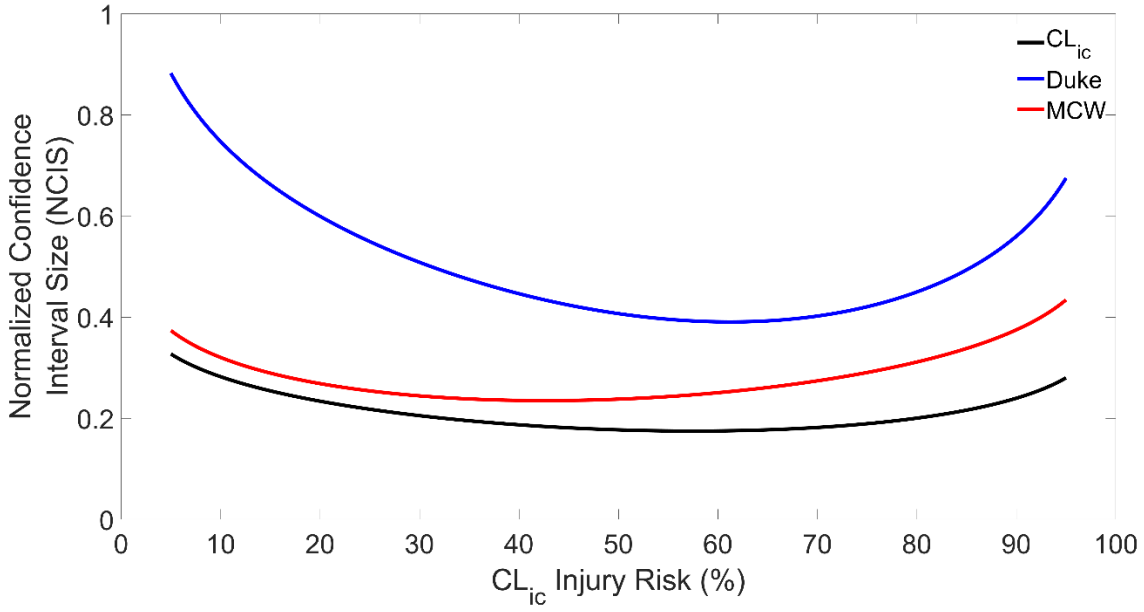

Figure 3-6: Normalized confidence interval size (NCIS) for combined loading metric of integrated data set (black), sagittal resultant axial force of n = 32 for Duke (blue) and n = 43 MCW (red). Note that the integrated data set (n = 75) optimizes the size of the confidence interval when compared to either of the force-based criteria across all injury risk probabilities (Ortiz-Paparoni et al., 2021).

A selected range of risk values of the IRC metric for Duke and MCW's force injury criteria are provided in

Table 3-3 and Table 3-4 respectively. In Figure 3-6 it is worth noting that the higher number of specimens for the MCW force injury criteria results in enhanced confidence intervals (red line) when compared to those of Duke (blue line). However, increasing the total number of specimens by combining the two data sets results in an improved confidence interval across all injury risk values (black line).

Table 3-3: Selected range of IRC values for the T12-L1 Resultant Force (F_r) for Duke's data set (Ortiz-Paparoni et al., 2021).

Risk Level	F_r (KN)	Lower 95% CI (KN)	Upper 95% CI (KN)	NCIS
0.05	2.23	1.45	3.42	0.88
0.1	2.61	1.81	3.76	0.75
0.2	3.16	2.35	4.24	0.60
0.3	3.62	2.82	4.66	0.51
0.4	4.07	3.26	5.08	0.45
0.5	4.54	3.71	5.56	0.41
0.6	5.07	4.17	6.16	0.39
0.7	5.70	4.67	6.96	0.40
0.8	6.54	5.23	8.17	0.45
0.9	7.91	6.00	10.43	0.56
0.95	9.26	6.65	12.89	0.68

Table 3-4: . Selected IRC values for the T12-L1 Resultant Force (F_r) for MCW's data set (Ortiz-Paparoni et al., 2021).

Risk Level	F_r (KN)	Lower 95% CI (KN)	Upper 95% CI (KN)	NCIS
0.05	3.85	3.20	4.63	0.37
0.1	4.33	3.69	5.08	0.32
0.2	5.00	4.38	5.72	0.27
0.3	5.55	4.91	6.27	0.24
0.4	6.06	5.39	6.82	0.24
0.5	6.59	5.85	7.42	0.24
0.6	7.15	6.31	8.11	0.25
0.7	7.82	6.82	8.96	0.27
0.8	8.67	7.43	10.12	0.31
0.9	10.01	8.31	12.06	0.37
0.95	11.27	9.09	13.98	0.43

3.4 Discussion

In this chapter we propose a novel combined loading injury criteria for the human lumbar spine that was derived under similar principles as previous established cervical injury metrics (Eppinger et al., 1998). The CL_{ic} represents a robust injury assessment by allowing the integration of multiple data sets and providing a combination metric (κ) that accounts for the resultant sagittal force and the decorrelated bending moment across a nominal range of lumbar spine postures. The CL_{ic} combines three different data sets that result in an injury risk assessment based on 75 cadaveric responses, a sizeable data set in the injury biomechanics community.

The moment about the T12-L1 vertebral disc center was chosen as an initial moment translation point. For bending moments, however, the translation to this point does not identify the effective center for moment action. This is not essential for injury criteria using axial or resultant force alone, but for combined injury criteria, the use of the effective moment center at T12-L1 is necessary to avoid F_z correlated moments that do not provide additional stress from bending on the anterior or posterior surface of the functional spinal unit. In fact, the determination of the effective moment center for translation of the M_y component has a level of inaccuracy that, from a priori estimates, could be as large as 4-6 cm depending on the specimen. Errors in assessing the effective moment center increases the correlation between the F_z and M_y components, adding uncertainty to the determination of a combined loading injury criteria. In the current

testing with large axial force components, the use of the vertebral disc center for moment translation produces moments and axial forces that are well correlated, suggesting that they do not have an independent effect and that the effective moment center is not located at the center of the disc (Xia et al., 2010). Across the Duke and MCW dataset, these correlations are generally large (Figure 3-3), reflecting the attainment of predominantly vertical loading (where $F_z >> F_x$) relative to the spine. The majority of the tests show highly correlated data owing to differences between the effective moment arm location and the assumed arm in the middle of the T12-L1 intervertebral disc. To decorrelate these, an additional antero-posterior translation of the moment arm was optimized to minimize the correlation between F_z and M_y over the loading phase of the test, which led to translations as high as 6.7 cm posterior to the originally determined effective moment arm location (Figure 3-4). All the optimized moment arm translations resulted in a shift of the effective moment center of T12-L1 in the antero-posterior direction towards the spinal canal. These moment arms allowed the determination of a decorrelated bending moment response at T12-L1 that was necessary to investigate the influence of an independent M_y response through a combined loading injury criterion. Decorrelation of M_y by translating the center of rotation in the antero-posterior direction produced independent effects on stress from M_y and F_z. The resulting values are also more biomechanically plausible since previous estimated M_y values higher than 250 Nm were not expected in predominantly axial loading.

The investigated distribution functions had similar Anderson-Darling coefficients (Table 3-1), with the Lognormal distribution improving the confidence intervals at the beginning of the injury risk curve (values below 20% injury risk) and towards the end of the curve (values above 80% injury risk). Additionally, the lognormal distribution has been reported in the literature by Yoganandan et al. (2020) to be a good representation of thoracolumbar injury risk assessments. Therefore, the human injury risk curves for both a combined and axial loading criteria were determined by means of a Lognormal distribution. The axial force only metric was similar when using the axial force (F_z) and the resultant force (F_r) independently (Figure 3-5). This is to be expected since, to mimic UBB loading scenarios, the tests conducted seek to replicate a mostly axial underbody loading pattern resulting in a sagittal resultant force with dominant axial (F_z) component. For the combined Duke and MCW data set the antero-posterior force (F_x) did not substantially increase the effective load on the specimens, with a $(F_r - |F_z|)/F_r$ ratio less than 5%. The Duke resultant sagittal force injury criteria resulted in a 50% risk of vertebral body fracture at 4.54KN (

Table 3-3), which was conservative with respect to MCW's resultant sagittal force at 6.59KN for a 50% injury risk (Table 3-4).

The combined metric (CL_{ic}) (Figure 3-5) derived from interval censored data using the T12-L1 resultant force and bending moment is recommended for vertebral body fracture for postures within one standard deviation of the nominal posture from the UMTRI seated soldier study (Reed and Ebert, 2013). This combined loading metric considers the bending moment effects allowing the inclusion of a range of thoracolumbar postures within the injury metric. This capability becomes valuable in the risk assessment of both a restricted range of seated posture loading conditions and postures into which the thoracolumbar spine can shift to during the course of an UBB loading event. In the investigated data set, the bending moment contributes only a minor portion to the stress to failure for the current tested spinal postures. The evidence for this is the optimization of the injury criterion to a large $M_{y,crit}$ value, which reduces the contribution of moment relative to compressive force in the injury assessment. It is anticipated that dynamic data with larger bending moment values relative to axial force will reduce $M_{y,crit}$ resulting in a higher influence of the bending moment in the expanded injury criteria. By allowing the integration of different data sets, hence increasing the number of investigated specimens, this combined loading metric results in lower uncertainty when compared to a force-based analysis (Figure 3-6). This combined loading metric represents a framework that may become the generic metric that can be used for injury predictions in general dynamic

loading. The combined metric is the first broadly applicable injury risk for thoracolumbar vertebral body fracture for a spine positioned in a nominal range of seated postures subjected to UBB conditions. The lumbar injury criteria (CL_{ic}) resulted in a combined metric value κ of 1 for 50% risk for a vertebral lumbar fracture, with 0.59 and 1.70 representing the 5% and 95% injury risk respectively (Table 3-2).

Limitations include a relatively restricted range of dynamic force/moment ratios. Chapter 4 will expand the range of postures evaluated to develop an injury criterion for postures with a wider range of M_y input conditions. Also, this study does not include assessments of other injury criteria outcomes such as injury to intervertebral disc or spinous processes. The human cadavers used for this study may have altered injury tolerance based on age related disc degeneration and other effects. So, caution should be exercised when applying the CL_{ic} to younger and healthier populations. It should also be noted that the reported CL_{ic} application is limited within the stated parameters of the investigated data set. The maximum decorrelated moment in this data set was 347 Nm, therefore, the applicability of this injury criteria should be restricted to scenarios with less than 347 Nm of decorrelated lumbar M_y. Similarly, the maximum M_y/F_r ratio in the current data set was 0.06 Nm/N, hence the recommended applicability of this CL_{ic} is within scenarios below that threshold. Shear forces did not substantially increase the effective load on the specimens in the current dataset. Therefore, the recommended applicability of this CL_{ic} is to scenarios where the $(F_r - |F_z|)/F_r$ ratio is less than 5%. Nevertheless, the

novel method developed in this work generalizes for sagittal combined loading scenarios where contributions from these components may be substantial given tests in an expanded range of bending moments or shears.

Though lateral and torsional bending scenarios may be common in current military vehicles, this injury criterion does not apply to either lateral or torsional bending and should not be used with transverse forces (e.g., F_y), lateral bending moments (e.g., M_x) or torsional bending moments (e.g., M_z). Since these scenarios are likely important in the presence of added torso supported mass, extension of the current injury criterion to lateral bending scenarios should be considered for future work. Finally, pure flexion and pure extension moments to failure, at least quasistatically, are not the same. This analysis assumes that the effects are the same or are of similar magnitude. Finally, current testing is predominantly in the compression half-plane. Therefore, the current injury criterion should not be applied in the tension half plane.

4 Expansion of the Combined Metric

Chapters 2 and 3 investigated the injury tolerance for the lumbar spine during UBB events to the axial force and a combined loading metric for a limited range of occupant's seated postures. However, it is highly desirable to expand the criterion to consider a wider range of postures with flexion and extension of the lumbar spine. Therefore, the objective of this chapter is to expand the previously established lumbar combined injury criteria (CL_{ic}) to encompass a wider range of seated postures and account for a higher contribution of the bending moment to the loading scenario. An expanded combined loading injury criterion (ECL_{ic}) was developed by incorporating 15 specimens tested in postures that further increased the extension or flexion of the lumbar spine to the 75 previously tested specimens in the nominal posture range.

4.1 Introduction

Determining the human injury tolerance of the lumbar spine has been a vital step for the development of effective underbody blast (UBB) injury mitigation efforts, such as the Warrior Injury Assessment Manikin (WIAMan) Army-sponsored initiative (Loftis et al., 2021). In theater data suggest that lumbar spine injuries are the 2nd most prominent injury occurring in vehicle occupants killed in action during an UBB event (Loftis et al., 2019). During an UBB event the rapid compressive loading of lumbar spine components can be coupled with bending moments depending on the occupant's seated position and weight distribution (Spurrier et al., 2016), which can then exacerbate the injury outcome

(Yoganandan et al., 2015b). While recent studies have determined an injury tolerance of lumbar vertebral body fracture due to axial compression alone (Yoganandan et al., 2020b), injury risk is highly dependent on the complex geometry of the spine and the loading path, which is likely not purely axial in most scenarios. Ortiz-Paparoni et al. (2021) addressed this issue by establishing a combined injury criterion, considering both axial force and bending moment for nominal seated postures and postures within one standard deviation of nominal determined through the UMTRI seated solider study (Reed and Ebert, 2013). However, it is highly desirable to include a criterion that considers a wider range of postures with increased bending moment to fully capture the potential injury risks.

4.2 Materials and Methods

To expand the range of assessed seated postures fifteen unembalmed cadaveric lumbar spines in four new postures were added to the 75 specimens discussed in chapters 2 and 3. As with the previous specimens, the lumbar spines were fixed to aluminum cups using poly methyl methacrylate (PMMA) and a high-density urethane at the proximal (T12) and distal ends (S1). The spines were oriented in one of four postures: ACU reclined, intermediate, flexed reclined, and flexed nominal posture (Figure 4-1) derived from the seated soldier with Army Combat Uniform (ACU) study (Reed and Ebert, 2013).

The general test setup (Figure 4-2) included a proximal and distal six-axis load cell (MC5-6-5000; AMTI, Watertown, MA) with a 22.2 KN max load to measure axial compression forces and bending moments during loading. Multi-axis accelerometers with a range of 200 G (ADXL377, Analog Devices, Norwood, MA) were attached to the left face of the bottom potting cup, the left face of the top potting cup, and glued to the L3 vertebral body. Two strain gauges were used, (Model EA-06-062AQ-350/P or CEA-13-250UW-350 or C2A-06-062LW-350, VPG Micro Measurements, Wendell, NC) with one gauge glued to each of the L2 and L4 vertebral bodies. Twelve acoustic sensors (Mistras S9225, Physical Acoustic Corporation, 300–1800 KHz) were instrumented on the vertebral bodies of interest to assist with the assessment and timing of fracture. Four acoustic sensors were glued to the L1 vertebral body, and two were glued to the remaining vertebral bodies (L2-L5). An internal LVDT (Serial number 227, MTS, Eden Prairie, MN) was used on the electro-servo-hydraulic mechanical test system (MTS) piston applying the displacement to the specimen. Finally, necropsy and micro CTs were performed after the last test on the specimen to determine injury outcome.

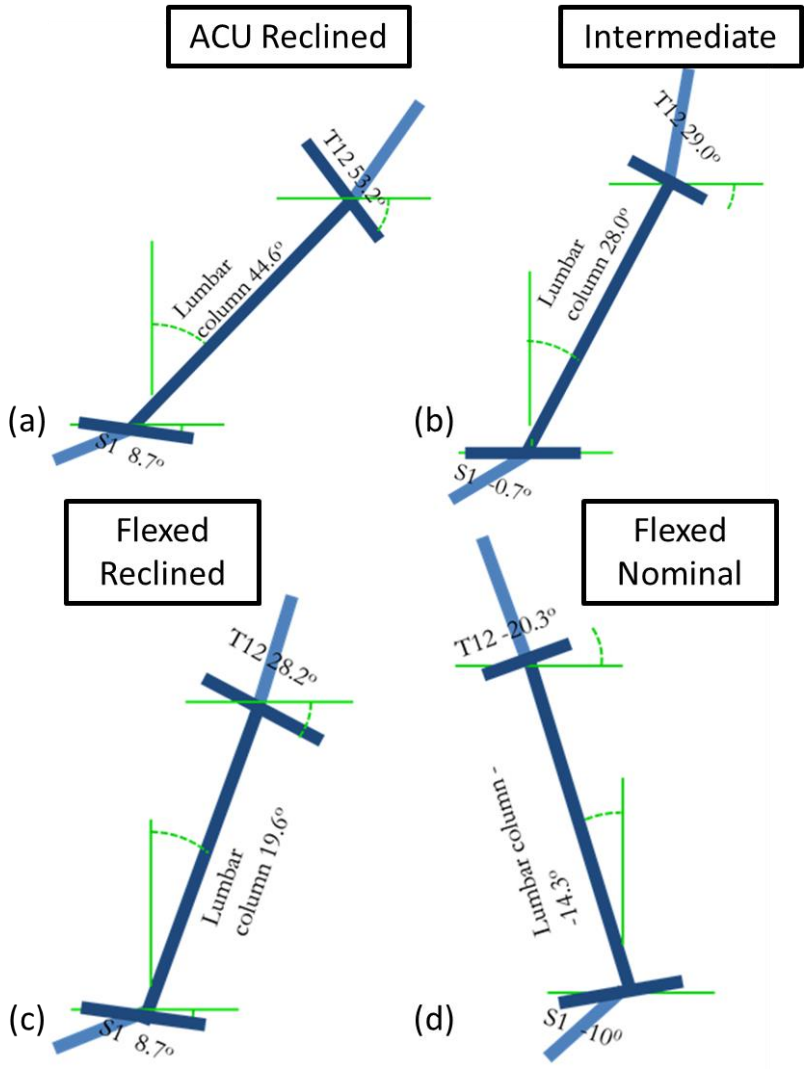

Figure 4-1: Expanded range of postures based on seated soldier. (a) ACU reclined. (b) Intermediate. (c) Flexed reclined. (d) Flexed nominal.

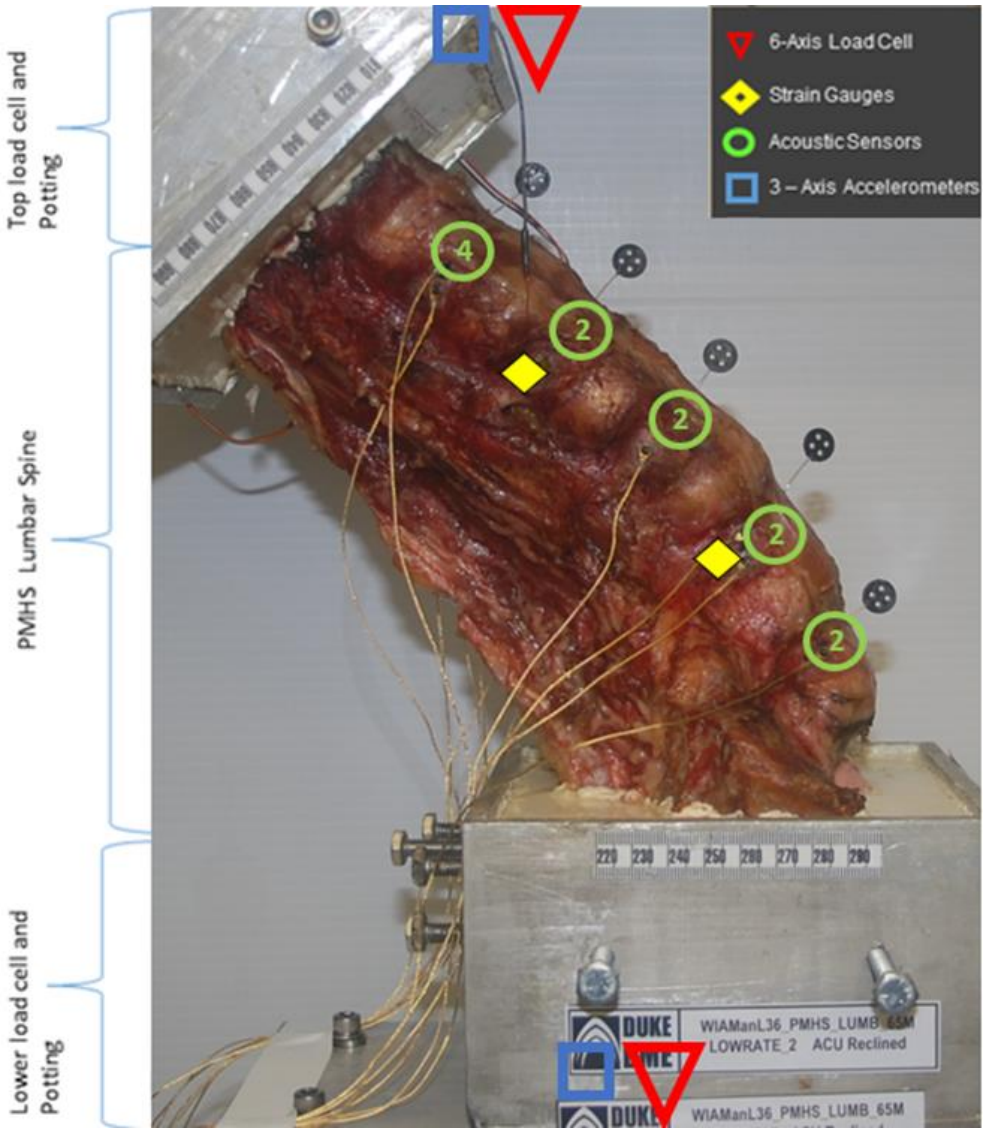

Figure 4-2: Test setup for LSPN36. The lumbar spine specimen is in the ACU reclined position and instrumentation has been identified

Signal collection, processing and analysis followed the procedures outlined in sections 2.2.1 and 2.2.3 of chapter 2. To maintain consistency across the experimental groups and allow a straightforward integration of the data sets, the expanded data set was subjected to the moment decorrelation procedure described in section 3.2.1 of chapter 3.

Further, the three proposed parametric distributions (Weibull, Loglogistic, and Lognormal) were also evaluated to determine the best representation of injury risk for the expanded combined loading injury metric (λ).

4.2.1 Combined metric optimization

As in chapter 3 the expanded combined loading metric (λ) was determined by optimizing a parameter of the parametric distribution. In this case the Anderson-Darling coefficient fit was selected as the optimization target over the minimization of the NCIS to ensure that the fit of the data was the primarily feature of the injury risk model. In a given test, the peak value of λ exists and it is given by $F_{r,crit}$ and $M_{y,crit}$. The critical values are ideally identified through tests with nearly pure axial loading and nearly pure moment loading which are not currently known for the proposed test conditions. However, the optimization of the AD coefficient allows the determination of the critical values by first starting with an initial approximation of the critical values, followed by a calculation of λ for the failure tests. Then a λ metric is calculated for known non-failure points based on acoustic and strain gauge data and a risk function is derived from the parametric distribution based on interval censoring using the previously identified injury and non-injury points. The AD coefficient is evaluated for the resulting distribution and then $F_{r,crit}$ and $M_{y,crit}$ are optimized through a line search algorithm until the AD coefficient is minimized.

4.2.2 Alternative weightings for the expanded range data

Since the new expanded posture tests (15) comprise a fraction of the total number of tests (90), weightings were explored to determine if the effect of the new tests was qualitatively different than the existing tests. To perform this analysis, the new tests were weighted up to 5 times (5X) the value of the old tests to make the new tests numerically equal to the old.

4.3 Results

A total of fifteen tests were performed in the expanded posture range, 4 in each of the ACU reclined, flexed reclined, and flexed nominal postures, and 3 in the intermediate posture. The tests resulted in 13 single or multi-level vertebral body fractures and 2 resulted in different injury types (Table 4-1). The fifteen specimens had a mean age, weight, height, and BMI of 64 ± 9 years, 80 ± 17 kg, 175 ± 7 cm, and 26 ± 4 kg/m^2. The expanded posture tests brought the total sample size of this study to 90 specimens and resulted in specimens that were 66 ± 10 years, 80 ± 13 kg, 177 ± 6 cm, and 26 ± 4 kg/m^2. Representative metric values (F_z, F_x, F_r, M_y) for the initiation of fracture and at maximum axial force were determined as described in section 2.2.3 of chapter 2 and are given in Table 4-2.

Table 4-1: Injury outcome from the 15 specimens of the expanded posture test series. ACUR denotes ACU reclined, FN denotes flexed nominal, I denotes intermediate, FR denotes flexed reclined.

Test ID	Posture	Vert fx	Injury description
LSPN33	ACUR	0	L1-L2, L2-L3, L3-L4 and L4-L5 IVD NP crush; L4 right superior articular facet fx
LSPN34	ACUR	1	T12 vertebral body fx, inferior endplate fx; L1 superior endplate failure; L1 right superior facet fx
LSPN35	ACUR	1	L1 vertebral body burst; L4 right superior facet fx
LSPN36	ACUR	1	T12 vertebral body fx; L2 vertebral body fx, NP intrusion to L2 inferior endplate; L2-L3 IVD rupture; L1 spinous process tip fx, L1 posterior left superior facet fx; S1 right ala superior tip fx
LSPN37	FN	1	L1 inferior endplate fx; T12-L1 and L1-L2 IVD crush; S1 endplate injury, major posterior sacrum fx
LSPN38	FN	1	T12 inferior NP intrusion; L1 vertebral body burst, L1 superior left facet fx, L1 inferior endplate failure; L2 vertebral body anterior-inferior fx, L2 tip of spinous process fx, L2 inferior right facet fx, L2 superior NP intrusion; L3 spinous process fx; L5 inferior endplate failure; S1 vertebral body fx, bilateral ala fx
LSPN39	FN	1	L1 vertebral body fx, L1 obliteration of neural arch, L1 bilateral pedicle fx, L1 superior endplate damage, L1 left transverse process fx; L2 vertebral body crush, L2 right pedicle fx, L2 left inferior facet fx extending to lamina; L4 right transverse process fx from facet with separation, L4 right inferior endplate fx; L5 left inferior anterior endplate fx; S1 endplate failure with NP intrusion, right posterior ala fx at cast
LSPN40	FN	1	L4 spinous process fx; L5-S1 IVD shear
LSPN41	I	1	T12 vertebral body fx, T12 ALL tear; L1 bilateral transverse process fx
LSPN42	FR	1	L3 bilateral pedicle and lamina fracture, completely separated, L3 bilateral superior articular process fx; L4 anterior vertebral body fx; L5 bilateral lamina fx, completely separated; L5-S1 right anterior inferior IVD burst; S1 right anterior minor vertebral body fx
LSPN43	FR	1	L2 vertebral body burst, L2 bilateral inferior facet joint capsule rupture
LSPN44	FR	1	L1 vertebral body burst; L5 major bilateral lamina fx with neural arch separation
LSPN45	FR	0	T12 neural arch fx
LSPN46	I	1	T12 anterior vertebral body fx; L3 left transverse process fx; L4 spinous process fx; L5 shear, bilateral pedicle, transverse process, superior facets; L5-S1 IVD shear
LSPN47	I	1	T12 vertebral body burst; L1 vertebral body burst; L4 spinous process fx

Table 4-2: Summary of combined Fr and Fz based peak values at the center of the T12-L1 IVD for the expanded test series. NA denotes non-failure test values for acoustic fracture identification. Note that the upper and lower bounds of the interval censored data are defined by the value at peak force and the value at the fracture initiation respectively. Specimens that did not present vertebral body fractures were designated as right censored.

Test ID	Value at Peak Axial Force				Fracture Initiation (Acoustic + Strain Gauge Onset)				Vert fx
	F_z (N)	M_y (Nm)	F_x (N)	F_r (N)	F_z (N)	M_y (Nm)	F_x (N)	F_r (N)	
LSPN33	4477	103	3508	5688	-	-	-	-	0
LSPN34	3211	54	1886	3724	2803	41	2393	3686	1
LSPN35	4850	23	3450	5952	3873	33	4048	5603	1
LSPN36	3490	18	2068	4057	2796	22	2389	3678	1
LSPN37	3694	2	1774	4098	NA	NA	NA	NA	1
LSPN38	6626	5	2583	7112	5199	138	1572	5432	1
LSPN39	7006	138	1882	7255	6933	114	2009	7219	1
LSPN40	5866	134	1339	6016	4513	111	1267	4688	1
LSPN41	4473	76	4126	6085	NA	NA	NA	NA	1
LSPN42	5967	66	2708	6553	5581	92	1348	5742	1
LSPN43	7395	28	2045	7673	6205	29	2014	6524	1
LSPN44	4732	69	1462	4952	4663	61	1498	4898	1
LSPN45	7958	206	3609	8738	-	-	-	-	0
LSPN46	7030	17	3012	7648	6673	121	4018	7790	1
LSPN47	6794	11	3096	7466	6475	84	3537	7378	1

4.3.1 Moment decorrelation

Compared to the nominal range of posture previously evaluated, the expanded data set presented lower correlation values between the axial force and bending moment (Figure 4-3). Decorrelation of M_y by translating the center of rotation in the antero-posterior direction towards the effective center of motion allowed the evaluation of

independent effects on stress from M_y and F_z. Displacements for the moment decorrelation are shown in Figure 4-4.

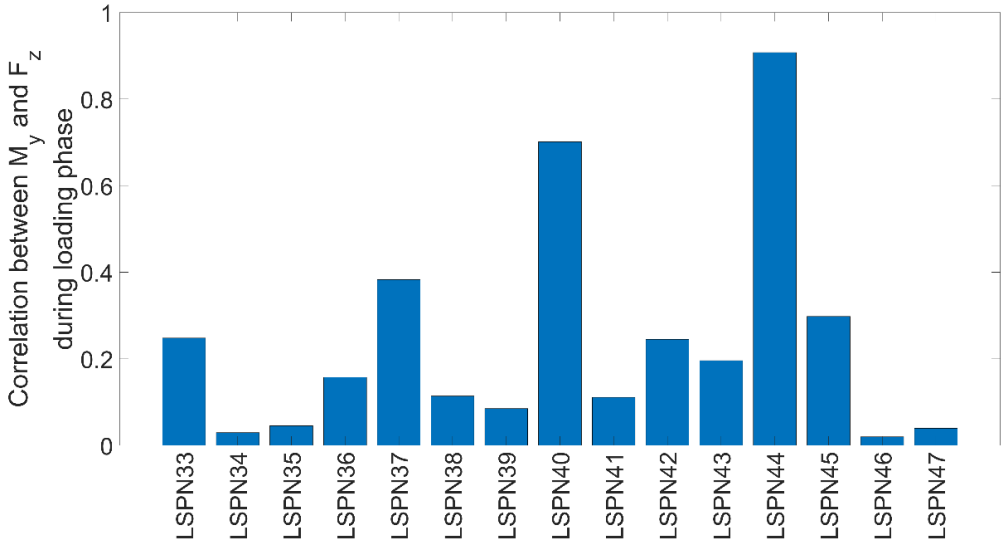

Figure 4-3: Correlation of Fz and My for 15 expanded range Duke lumbar tests. Correlations between axial force and moment are generally smaller for the more off-axial tests (ACU Reclined and Intermediate). Correlations are generally lower than those in the previous 75 nominal posture range.

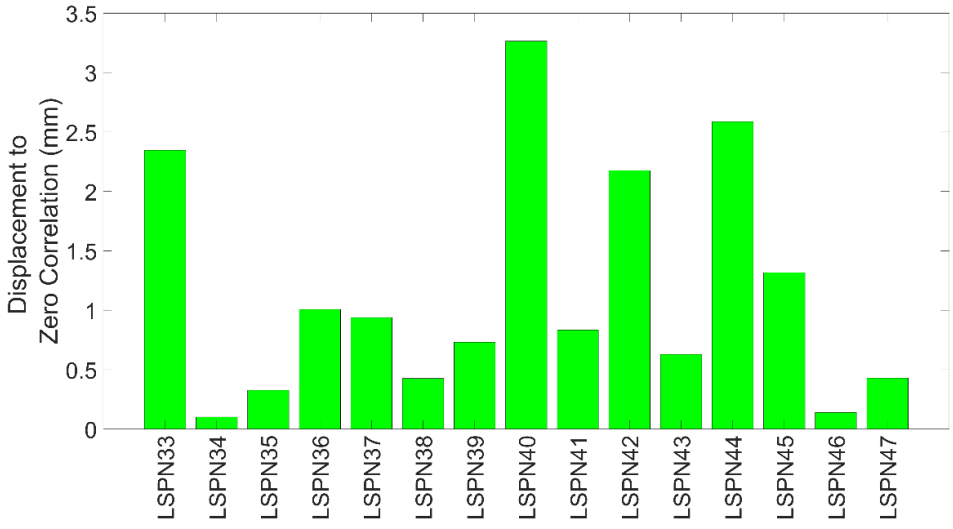

Figure 4-4: Posterior translations to the effective center of rotation that minimize correlation between F_z and M_y for the expanded data set.

4.3.2 Expanded combined loading metric

The optimized AD fit coefficients for the parametric distributions evaluated are given in Table 4-3. From these results a Loglogistic distribution was selected as the best representation of injury risk, resulting in optimized critical values of $F_{r,crit}$ = 6011 N, and $M_{y,crit}$ = 904 Nm, with location (μ) and scale (σ) parameters equal to 0 and 0.1797 respectively. The Loglogistic injury risk (Figure 4-5) is given by equation 4.1 and selected values of the injury risk are given in Table 4-4.

$$ECL_{ic} = \frac{1}{\left(1 + exp\left[-\frac{\ln(\lambda) - \mu}{\sigma}\right]\right)} \tag{4.1}$$

Table 4-3: Optimized Anderson-Darling (AD) coefficients for the parametric distributions evaluated.

Metric	Distribution	AD
$ECL_{ic}(\lambda)$	Weibull	0.918
$ECL_{ic}(\lambda)$	Loglogistic	0.422
$ECL_{ic}(\lambda)$	Lognormal	0.517

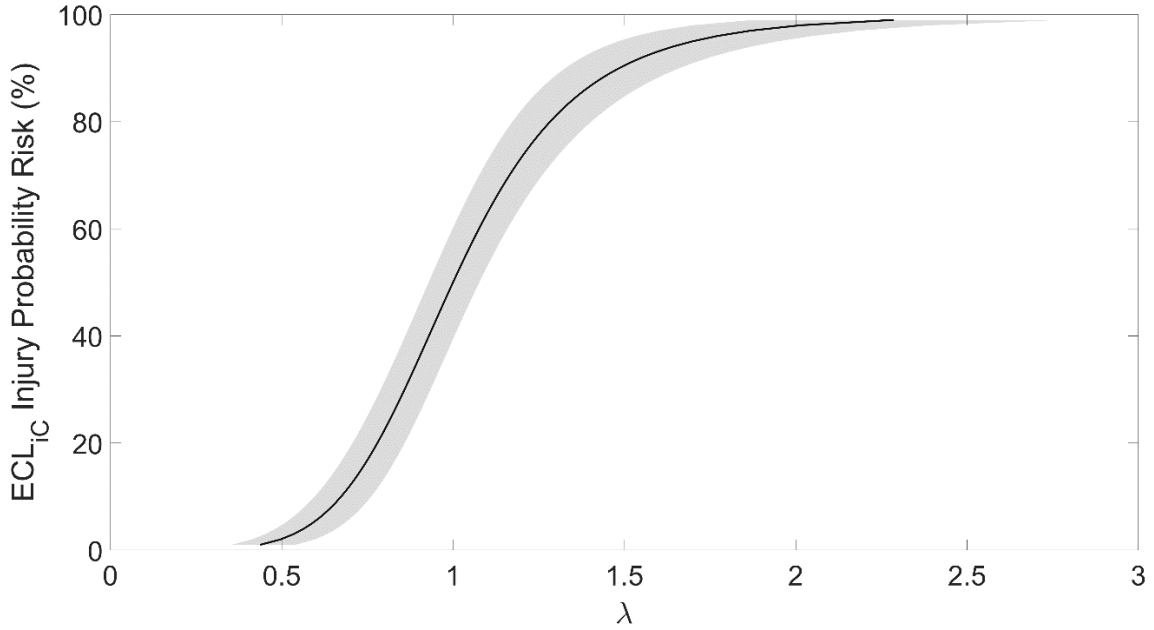

Figure 4-5: Lumbar spine vertebral body fracture injury risk for the expanded range of postures. The combined metric λ consists of a combination of the T12/L1 resultant force and moment fitted to a Loglogistic distribution (center black line) with 95% confidence intervals (shaded area).

Table 4-4: Selected injury risk values for the T12-L1 resultant force and moment combined loading metric (λ).

Risk Level	λ	Lower 95% CI	Upper 95% CI	NCIS
0.05	0.59	0.51	0.68	0.30
0.1	0.67	0.60	0.76	0.24
0.2	0.78	0.71	0.86	0.19
0.3	0.86	0.79	0.93	0.17
0.4	0.93	0.86	1.00	0.15
0.5	1.00	0.93	1.08	0.15
0.6	1.08	1.00	1.16	0.15
0.7	1.16	1.08	1.26	0.16
0.8	1.28	1.17	1.40	0.18
0.9	1.48	1.33	1.66	0.22
0.95	1.70	1.48	1.95	0.27

4.3.3 Alternative weighting

Anderson-Darling coefficients for 5X augmented data set fit (Figure 4-6) indicate that the statistical fit tests improve with the new weightings for all the distributions evaluated. The NCIS also qualitatively improves with the 5X weighting (Figure 4-7). In contrast, the effect of the 5X analysis on the mean risk is minimal (Figure 4-8).

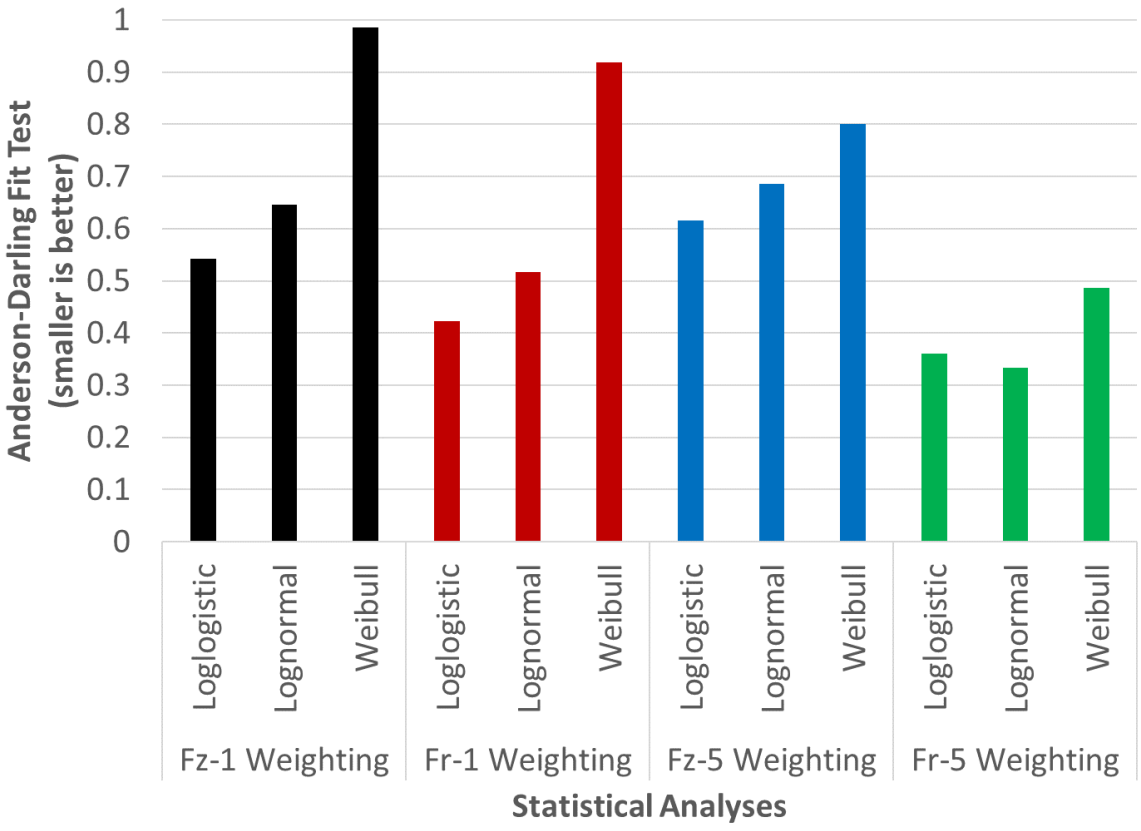

Figure 4-6: Anderson-Darling fit coefficients for various distribution and weighting values for F_z and F_r based injury risk models. As above, the Loglogistic distribution has generally better fit coefficients with the 5X fit generally better than the 1X fit.

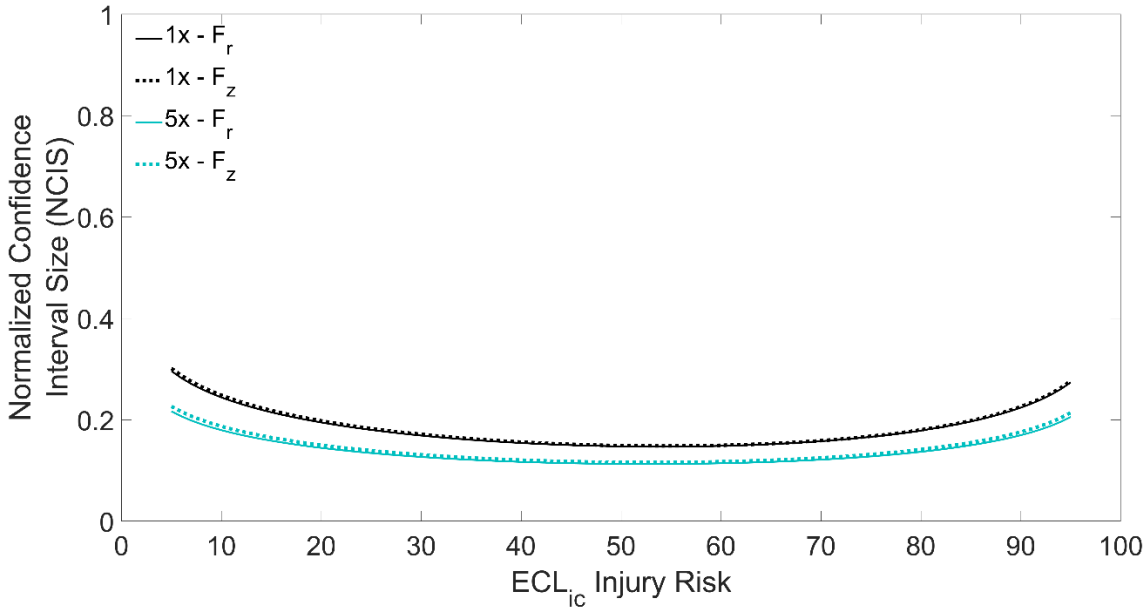

Figure 4-7: NCIS values for Loglogistic distribution for F_z and F_r based injury risk models. The 5X analysis is generally better than the 1X analysis.

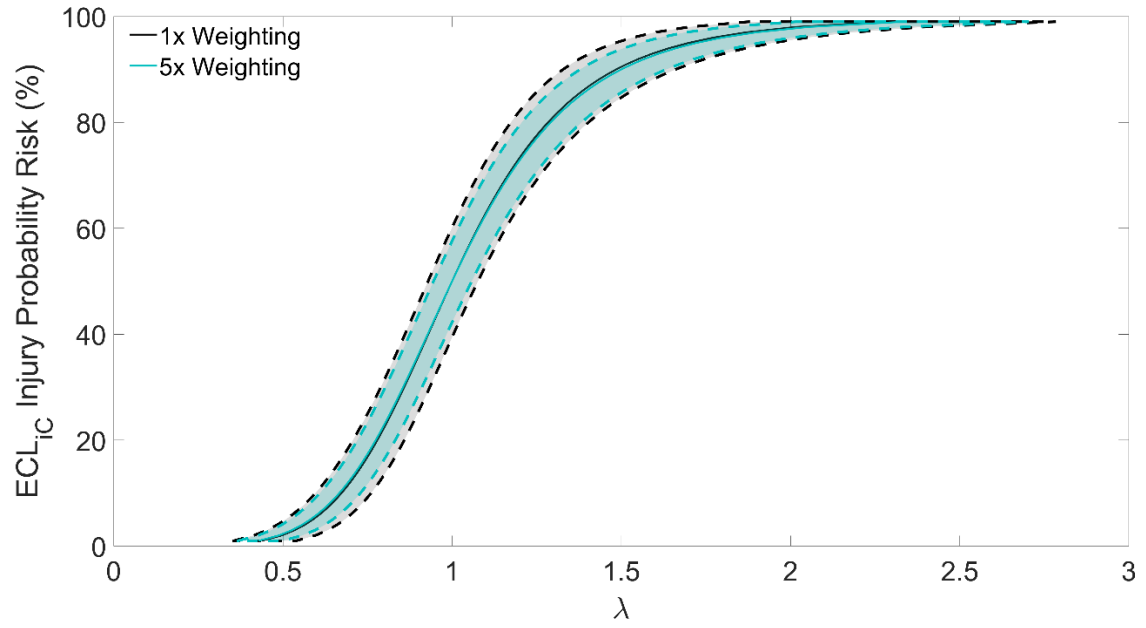

Figure 4-8: Loglogistic injury risk for 1x and 5x weigthing. The mean curves for F_r – 5X and F_r – 1X weighted are indistinguishable at this scale though the 5X confidence intervals are improved in the 5X analysis.

4.4 Discussion

The objective of this study was to expand the range of applicability of the lumbar spine combined loading injury criterion (CL_{ic}) presented in chapter 3. The analysis methods followed best practices in the injury biomechanics community and maintained continuity with the previously developed criterion.

A new range of postures that increased the flexion/extension of the lumbar spine (Figure 4-1) was included to the expanded criterion (ECL_{ic}) and augment its applicability within the seated soldier environment. The combined metric using the sagittal T12/L1 resultant force and moment was the recommended metric to evaluate vertebral body fracture risk and was extended beyond the one standard deviation of the seated soldier study nominal posture (Reed and Ebert, 2013).

The bending moment contribution in the expanded 15 specimens presents a higher contribution than that previously evaluated in the nominal posture range (L_{ic} $M_{y,crit}$ = 1155 Nm vs. ECL_{ic} $M_{y,crit}$ = 904 Nm). When combining the extended range of evaluated postures with the CL_{ic} injury criterion, the optimization of the Anderson-Darling coefficient for the ECL_{ic} development resulted in a smaller critical M_y value. This reduction highlights the expanded contribution of the bending moment to the one captured by the previously developed injury criterion. The combined metric represents a framework that may become the generic metric that can be used for injury predictions in general dynamic loading. The associated distribution function which best represented the data and had an

optimized Anderson-Darling coefficient was a log-logistic distribution (Table 4-3). While the expansion of the injury criterion provides valuable insights to the lumbar spine injury risk, it is important to note that the developed criterion assesses the risk of a single or multi-level vertebral body fracture occurs during a dynamic compressive event. Therefore, additional studies are needed to develop an injury probability risk for different injury types across multiple vertebral bodies, injuries to intervertebral disc or spinous processes.

In contrast with the previous axial-compression dominated data, the current dataset correlations between F_z and M_y are often small (Figure 4-3), reflecting relatively independent contributions to the stress state in the spine. As previously discussed in chapter 3, the majority of the nominal posture range tests show highly correlated data owing to differences between the effective center of rotation and the assumed center in the middle of the T12/L1 intervertebral disc. The lower distance to the effective center of rotation for the expanded data set (Figure 4-4), when compared to the nominal posture range, is in agreement with the smaller correlation observed between F_z and M_y for the expanded postures.

Due to the discrepancy in the number of specimens available between the nominal and expanded posture ranges (n = 75 vs. n = 15), alternative weighting for the expanded posture data set was explored (Figure 4-6). Overall, though there is an improvement in

NCIS in the 5X analysis (Figure 4-7), the lack of qualitative effect on the mean curve (Figure 4-8) suggests that the 1X analysis is a good representation of the range of postures included in this study and should be the analysis on which the injury criterion is based. The expanded combined metric (λ) of 1.0 represents a 50% chance of a single or multi-level vertebral body fracture (Figure 4-5). Approximately 1.7 and 0.59, represent a 95% and a 5% chance of the same injury, respectively.

While this work presents the first broadly applicable combined loading injury criterion for lumbar vertebral body fracture in a spine positioned in a range of seated postures subjected to UBB loading conditions, it is not without its limitations. Several of the CL_{ic} limitations, with some modifications, carry on to ECL_{ic}, these are:

- The maximum moment in the dataset was 487 Nm after minimizing the F_z - M_y correlation. Therefore, the strict applicability of this injury criterion is to scenarios with less than 487 Nm of M_y.

- The maximum M_y (Nm)/F_z (KN) ratio in the current dataset was extended from the nominal posture 0.06 to 0.1. Hence, the recommended applicability of ECL_{ic} can be expanded beyond a 0.06 M_y/F_z ratio but kept in scenarios where ratio is less than 0.1.

- The contribution of shear forces was increased in the current dataset. No limitations on the absolute value of F_x or F_z are recommended at this time. In

terms of contribution, the recommended applicability of this HIPC is to scenarios where the $|F_x|/F_r$ ratio is less than 25%.

- Though lateral bending scenarios may be common in current military vehicles, this injury criterion does not apply to lateral bending and should not be used with transverse forces (e.g., F_y) or lateral bending moments (e.g., M_x). Since these scenarios are likely important in the presence of torso supported mass, extension of the current injury criterion to lateral bending scenarios should be considered for future work.

- Though torsional bending scenarios may be common in current military vehicles, this injury criterion does not apply to torsional bending and should not be used with torsional bending moments (e.g., M_z). Since these scenarios are likely important in realistic loading in the presence of torso supported mass, extension of the current injury criterion to torsional bending scenarios should be considered for future work.

- Pure flexion and pure extension moments to failure, at least quasistatically, are not the same. This analysis assumes that the effects are the same or are of similar magnitude. It should be noted that the current testing is predominantly in the flexion/compression quadrant, hence the injury criterion should not be applied in the tension half plane.

5 The Energy Method

Methods used to develop an anthropometric test device (ATD) injury assessment reference curve (IARC) from a human injury probability curve (HIPC) such as matched-pair testing or perfect biofidelity, rely on the capability of the dummy to mimic the human behavior under the corresponding loading and boundary conditions. However, the degree of biofidelity is limited by constraints and design requirements; and matched-pair testing can result in an overestimation of the injury point due to intrinsic differences in both material behavior and performance to failure between the ATD and human. To ensure that the testing conditions between a cadaver and an ATD are comparable, this chapter proposes an energy equivalency method to translate the human injury response to an ATD injury assessment reference value (IARV) or an IARC. A generic axial force response was used to illustrate the generation of an IARC for a generic ATD through energy equivalency methods. To translate a single metric to the ATD IARC, the generic cadaver data set and the surrogate force-energy responses were generated to determine the transfer function from cadaver measurement to ATD measurements at iso-energy. Similarly, a generic response of a combined metric, similar to the combined loading injury criterion (CL_{ic}) developed in chapter 3, was used to illustrate the translation of a complex loading scenario by characterizing the energy response of both cadaver and ATD in the corresponding duplets that define the CL_{ic}.

An injury risk assessment (IARC) from actual ATD data has been performed using the techniques described in this chapter. The IARC was established for the WIAMan lumbar component and developed from the characterization of the experimental response of the ATD component to the seven lumbar orientations described in chapters 2 and 4. The lumbar component of the mannequin was tested in every orientation up to cadaver failure energies. The Human Injury Probability Curves (HIPCs) developed in chapters 2, 3 and 4 from 90 cadaveric specimens were then translated through the proposed iso-energy method to an IARC for the WIAMan lumbar component. The methodology, results, and final IARC was reported to the WIAMan project engineering office. However, owing to sensitivities regarding military dummy IARCs, the data used in this chapter to illustrate the iso-energy method are idealized and results are not based on any real ATD component data.

5.1 Single metric translation

Directly matching a single metric, for instance a force, for human and dummy responses leads to an incorrect measurement of the injury reference value due to the differences in mechanical work to failure between the human and the dummy (Figure 5-1).

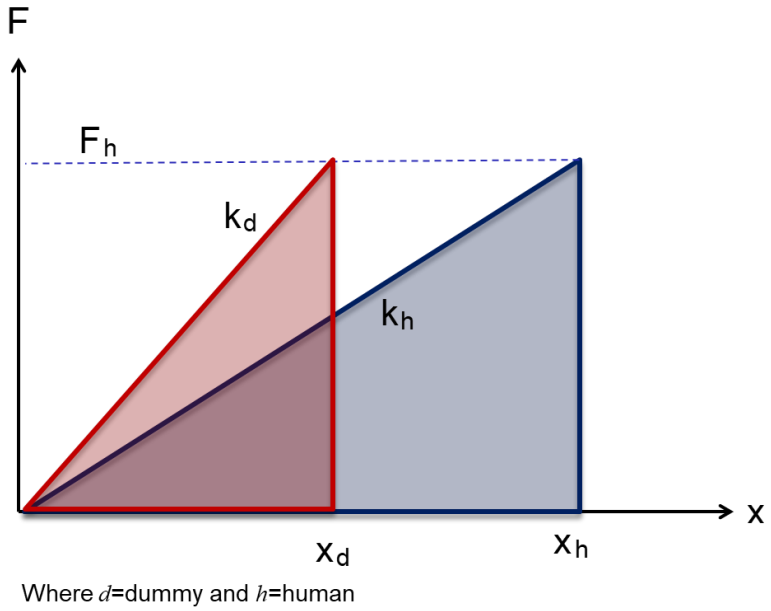

Figure 5-1: Linear elastic scaling at equal force. Note that the mechanical work (area under the curve) for the dummy and human differ at the same force value.

Similarly, when matched to failure displacement the mechanical work performed by the human and dummy is different (Figure 5-2). This linear stiffness scaling alone is not enough to capture the appropriate amount of energy that was introduced to the system to cause failure.

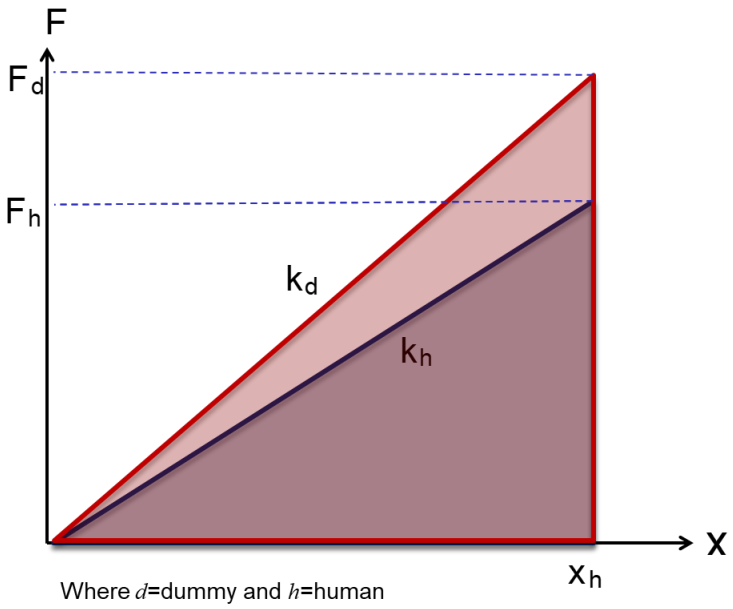

Figure 5-2: Linear elastic scaling at equal displacement. The mechanical work for the dummy and human differs.

Another critical limitation of commonly used matched-pair testing is the capability of the dummy to perform well beyond the cadaver fracture point (Figure 5-3). While matched-pair testing can allow a direct correlation of measured ATD responses to cadaver injury outcomes, the performance of the ATD beyond the cadaver fracture results in an overestimation of the injury tolerance as we do not expect the dummy to fail.

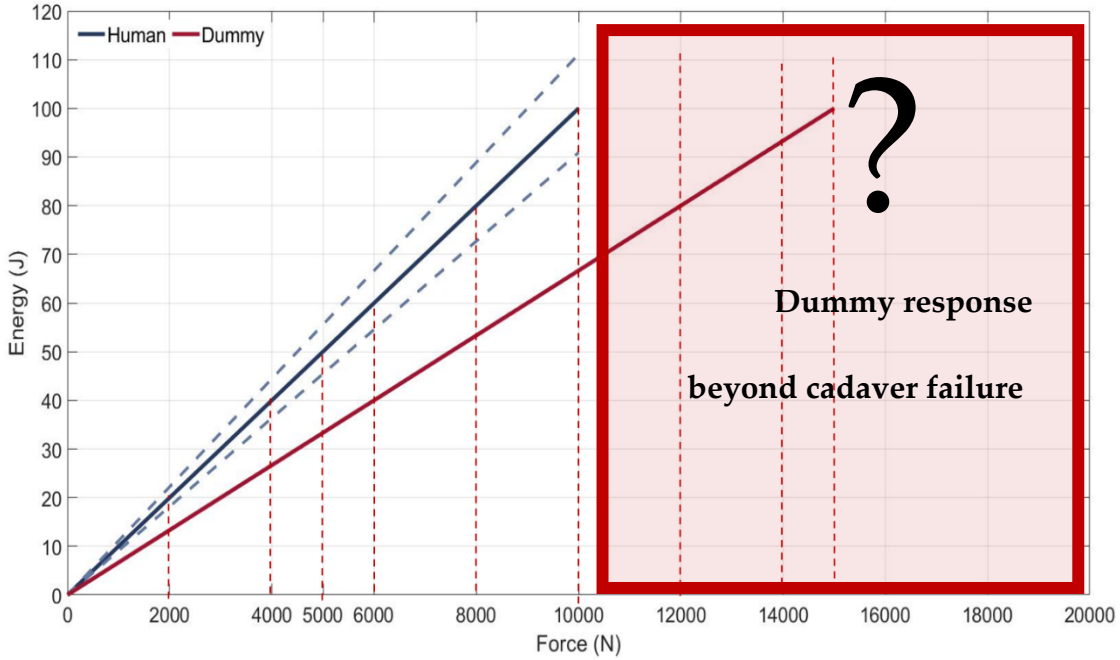

Figure 5-3: Linear elastic isoforce equivalency method on generic dataset for HIPC to IARC translation.

Another drawback to commonly used matched-pair testing for IARC generation is that the dummy, following design parameters, will not fail during the experimental run. Matching an equal velocity input between cadaver and ATD for injurious cadaver conditions will produce a failure in the cadaver, limiting the peak forces and moments beyond the failure point. In contrast, a nonfrangible ATD designed to have a much higher failure point, will continue increasing force/moment beyond the cadaver values, often designed to endure forces and moments far beyond human tolerance. So, even when the ATD is designed to match the human stiffness, the dummy will outperform the cadaver in an injury test of the same input (Figure 5-4, left) inevitably shifting the injury risk

assessment to the right and resulting in an overestimation of the injury tolerance (Figure 5-4, right).

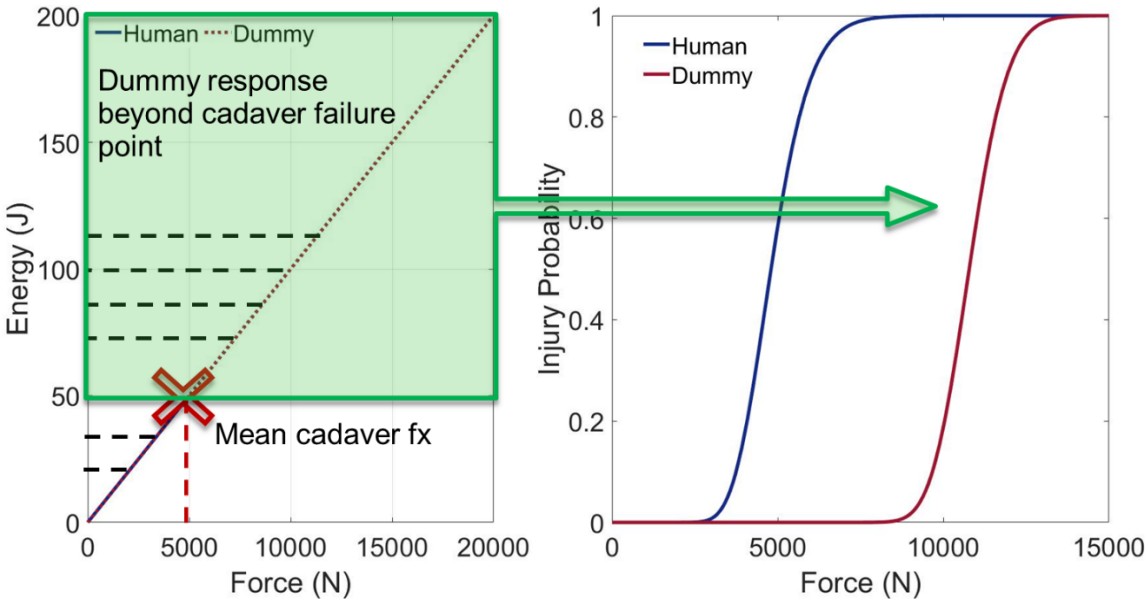

Figure 5-4: Force-Energy response and injury risk curve through the commonly used matched-pair method.

To overcome these limitations an energy equivalency method was proposed. The energy is the result of the scalar product of two vectorial quantities, the force and displacement (Equation 5.1), and as such it is independent of the system where it is determined (i.e., invariant) with:

$$E = \int F_z \cdot dz \tag{5.1}$$

where F_z is the upper load cell value (unaffected by acceleration) and dz is the incremental piston displacement measured by the LVDT. For a simple linear elastic scaling model:

$$F = k * x \tag{5.2}$$

$$E = \frac{1}{2}F * x = \frac{1}{2}\, k * x^2 \tag{5.3}$$

Equating for iso-energy scaling as defined by Figure 5-5:

$$E = \frac{1}{2}k_h x_h^2 = \frac{1}{2}k_d x_d^2 \tag{5.4}$$

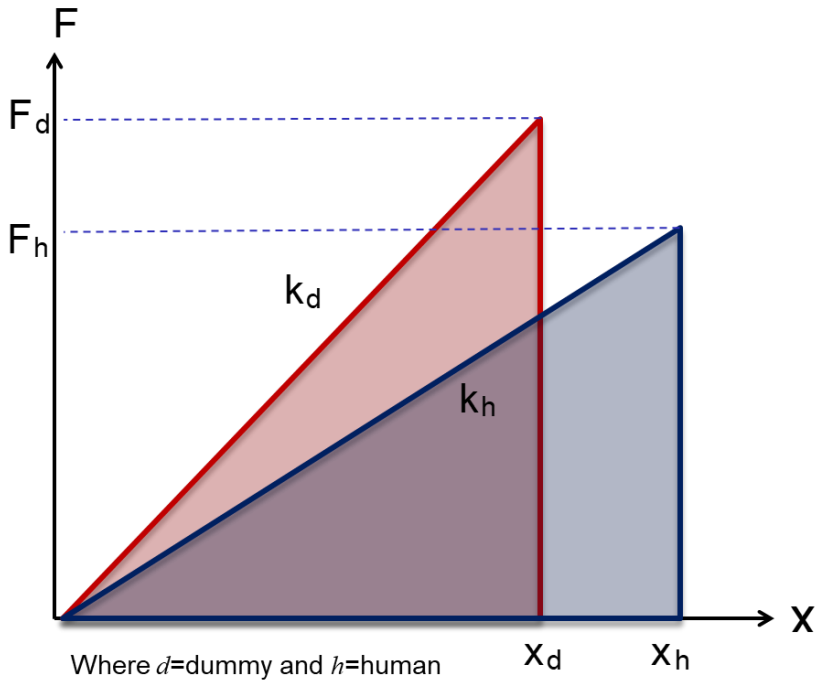

Figure 5-5: Scaling for a linear elastic model at iso-energy.

By characterizing the cadaver and ATD energy response in terms of force (Figure 5-6) we can determine the equivalent response between cadaver and ATD at iso-energy. The transfer function obtained during an iso-energy translation (Figure 5-7) can then be used to develop the ATD IARC by determining the corresponding injury points across the cadaver and ATD.

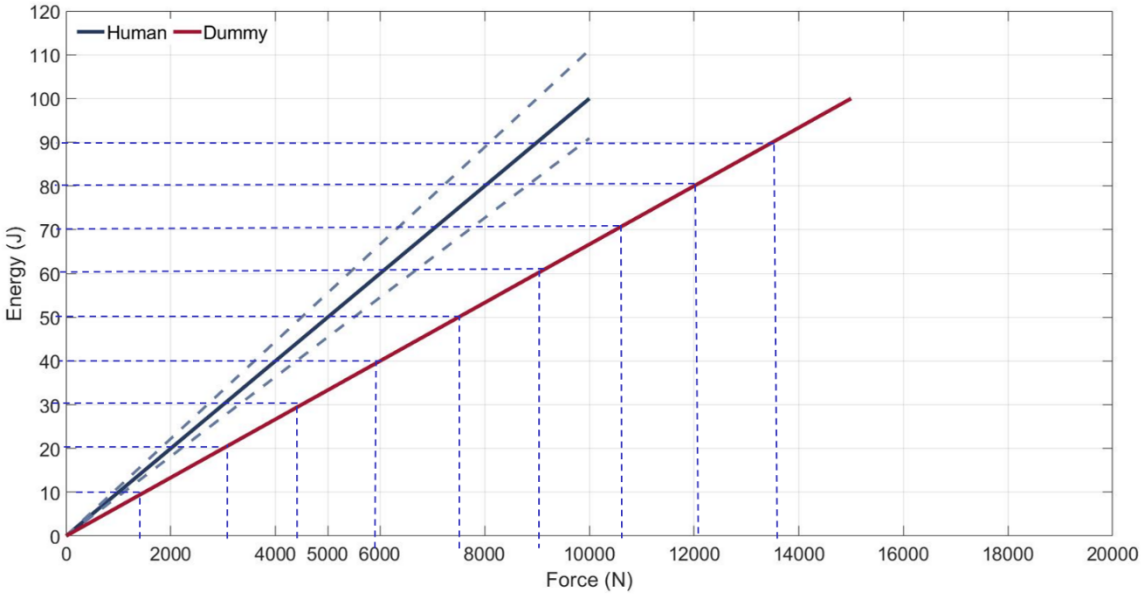

Figure 5-6: Linear elastic iso-energy equivalency of cadaver and ATD response on generic dataset.

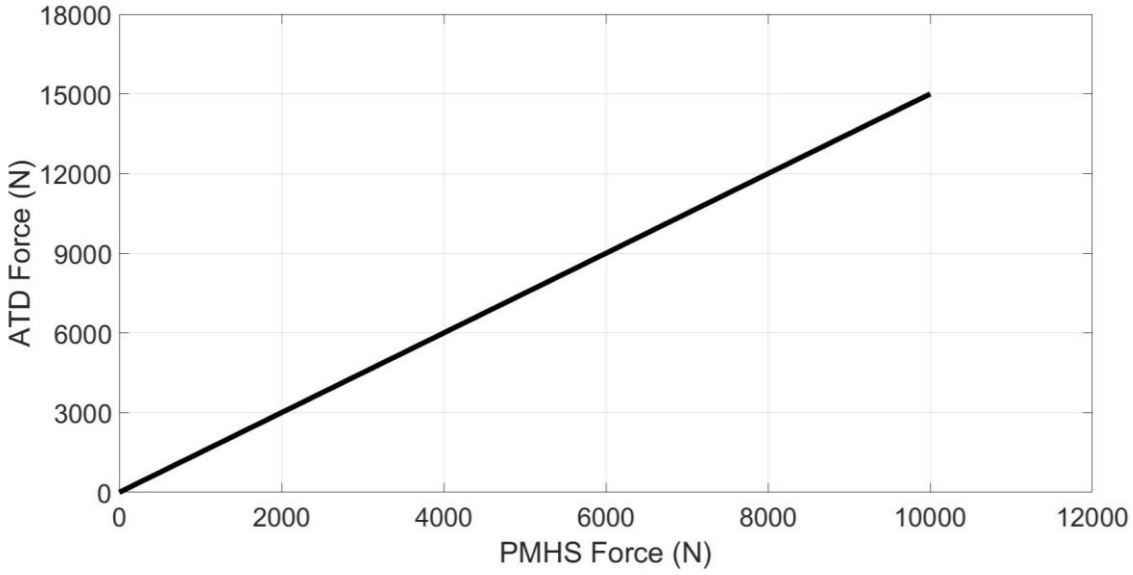

Figure 5-7: Cadaver to ATD transfer function at iso-energy for a generic dataset.

The injury risk (IARC) for the ATD can then be determine by matching the cadaver injury risk at a given force with the corresponding ATD force given by the iso-energy transfer function.

5.2 Combined loading metric translation

As in the energy equivalency of the force metric (Equation 5.4) the moment energy equivalency is defined as:

$$E_M = \frac{1}{2}\, b_h \theta_h^2 = \frac{1}{2}\, b_d \theta_d^2 \tag{5.5}$$

with the subindices *h* and *d* referring to the cadaver and dummy, respectively.

To account for the moment contribution to the system's energy, based on prismatic beam failure theory and as with the proposed CL_{ic} combined metric the energy of the system is defined as the sum of the force strain energy contribution and the moment strain energy contribution, defined as:

$$E = E_F + E_M = \frac{1}{2}\, k_h x_h^2 + \frac{1}{2}\, b_h \theta_h^2 = \frac{1}{2}\, k_d x_d^2 + \frac{1}{2}\, b_d \theta_d^2 \tag{5.6}$$

This is a point estimate for the energy, and both the displacements for the force (x_h) and the moment (θ_h) are estimated using cross head motion and geometric constraints. Since the cadaver and dummy are nonlinear, the strain energy for both force and moment are calculated using the point estimate in equation 5.6 by the integral form as:

$$E = E_F(t) + E_M(t) = \int \frac{1}{2}\, k_h x_h^2(t)dt + \int \frac{1}{2}\, b_h \theta_h^2(t)dt \tag{5.7}$$

$$= \int \frac{1}{2}\, k_d x_d^2(t)dt + \int \frac{1}{2}\, b_d \theta_d^2(t)dt$$

Since the cadaver energy contribution has been reduced to a single risk assessment parameter, κ as described above, there is an association between this value $\kappa(M_y, F_z)$ and energy based on equation 5.7.

To make the translation for the dummy in a manner analogous to the previous force-only injury assessments, a surface in three dimensions (F_z *or* F_r, M_y, E) is needed that describes all of the energy values for the dummy lumbar response as a function of force/moment pairs accessible during testing of dummy components. To perform the mapping from cadaver to dummy a surface in 3D was approximated using generic values for cadaver and dummy moment, force, and energy response. Energy values on this surface were assumed to correspond to the energy values represented in the cadaver CL_{ic} single parameter k. Thereafter, a 3D optimization was performed to find the energy from the cadaver CL_{ic} that corresponded to an F_z *or* F_r, M_y doublet from the dummy approximation surface plot. Note that this optimization produces a monotonically increasing energy line on the surface that provides the κ values for the dummy IARC.

The mapping was performed at iso-energy levels (Figure 5-8). It was assumed that the injury metric ratio (κ) behaved equally between cadaver and dummy response. At a given cadaver energy level the F_r/M_y ratio is defined through the average energy equivalent responses of the dummy to the expanded IARC.

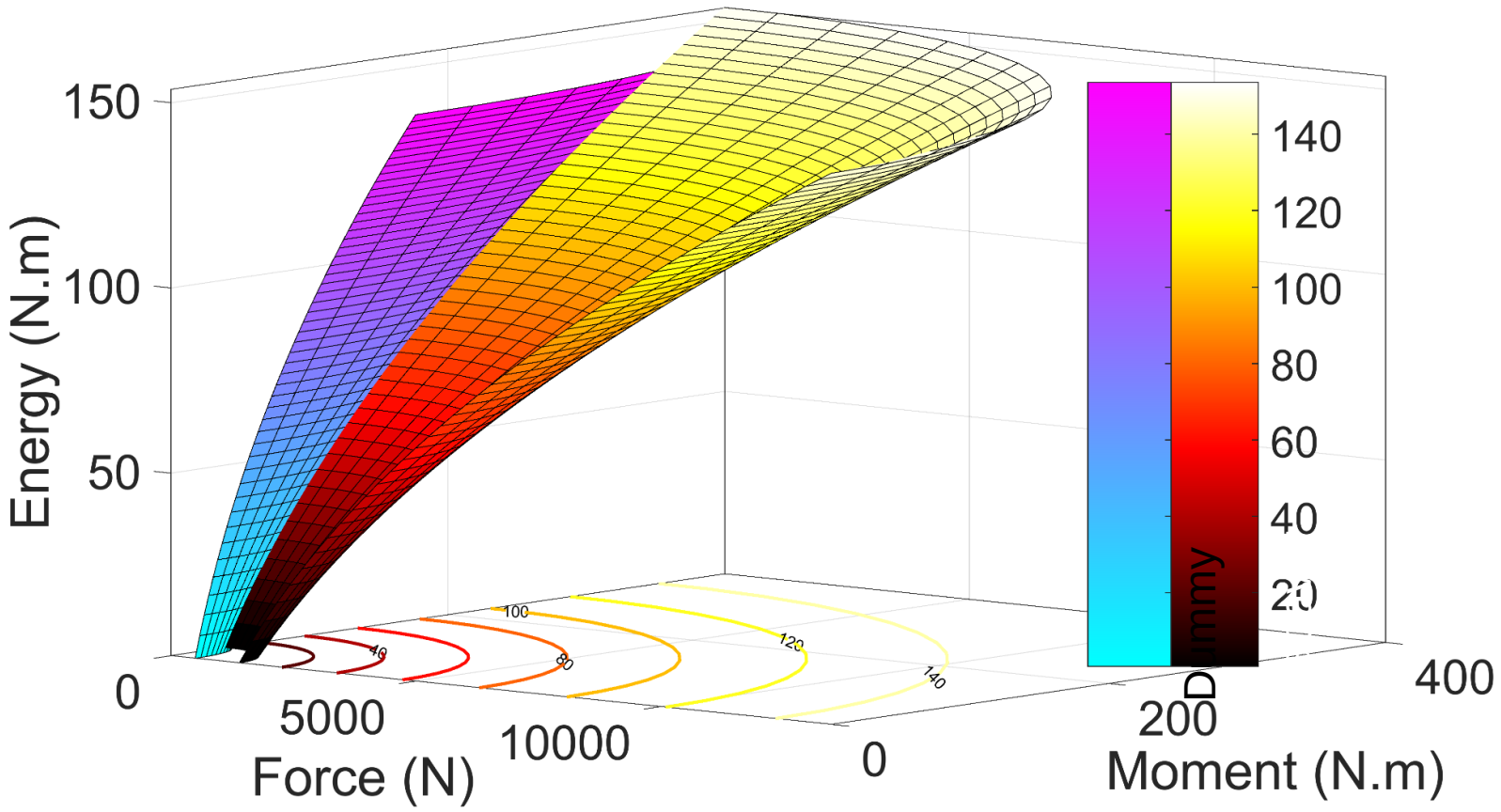

Figure 5-8: Example of surface plot of Force (F_z or F_r) and Moment (M_y) vs. Energy for cadaver energy response extrapolation.

6 Conclusions

Injuries to the lumbar spine during dynamic compression in soldiers have been highly prevalent in recent American military conflicts. Elucidating the injury risk of the lumbar spine during underbody blast scenarios is imperative for the advancement of protective equipment, and injury mitigation strategies. However, the literature still needs to catch up with the characterization and determination of injuries during UBB scenarios. While recent studies have shed light on some of the principal metrics that dominate the injury behavior of the lumbar spine under dynamic compression and proposed pertinent injury criteria, an expansion of the injury risk and its translation to real-world applications is needed.

This study proposed an axial injury criterion for three different seated soldier postures, with one of them in agreement with the injury criterion proposed in a recent study. Further, it introduces a combined loading metric criterion to account for the complex loading pattern of the lumbar spine during UBB by considering the bending moment contribution to the injury risk. Additionally, the combined metric was expanded beyond the initial three tested postures to inform its applicability in a wider range of seated postures. Finally, this study proposes a novel method based on energy equivalency to translate the experimental injury criterion to anthropometric test devices to advance the development of injury mitigation strategies.

6.1 Contributions and Impact

The work presented in this dissertation contains several contributions to the literature on lumbar spine injury under dynamic compression, expanding the current state of knowledge in the field.

The axial injury criteria developed in chapter 2 (L_{ic}) establishes the first injury tolerance values and injury risk functions for two postures that deviate one standard deviation from the nominal seated soldier posture. These axial criteria can be used to inform the tolerance to injury of the lumbar spine during life-fire testing, laboratory, and UBB environments. The injury criteria are relevant beyond the initial seated posture of the soldier, as it can be applied at any point during the compressive event were the lumbar spine shifts to the pre-flexed or pre-extended postures. The proposed criteria represent an important advancement in the development of anthropometric test devices, and injury mitigation strategies to reduce the incidence of lumbar spinal injuries in UBB scenarios. Another important contribution of the axial loading injury criteria is the significant differences that were observed between the nominal and the pre-flexed and pre-extended postures. A key suggestion from these differences is that the injury tolerance of the lumbar spine is not captured by axial data alone due to the difference in moment contributions across the three postures. Hence, it highlights the importance of introducing a combined loading metric that can capture the complexities of the loading path during the UBB event and its effects on injury tolerance on the lumbar spine.

A combined loading criterion for the cervical spine has been established in the past and is widely use in civilian automotive applications, policy regulation, and ATD calibration and certification. However, such criterion spine has yet to be proposed in the literature for the lumbar spine. The work presented in Chapters 3 and 4 provides the first combined loading injury criteria for the lumbar spine during dynamic compression conditions (CL_{ic}, ECL_{ic}). The ability to capture the contribution of the bending moment to the lumbar spine injury threshold allows for a better representation of the complex loading pattern of an UBB event and its effect on injury threshold. Further, the introduction of a combined metric allows the integration of datasets derived from different lumbar spine postures to result in an injury risk function derived from 75 cadaveric tests in the case of the CL_{ic}, which is a considerable sample size for human cadaveric testing. The size of the data set is further increased in the development of the ECL_{ic} outlined in Chapter 4 resulting in a total sample size of 90 cadaveric lumbar tests. Additionally, the applicability of the expanded combined loading criteria (ECL_{ic}) is also broadened to a wider range of postures that further extend or flex the lumbar spine, hence representing an increased range of seated soldier postures and positions into which the lumbar spine can shift during dynamic compression. Accounting for bending moment contribution, increasing the sample size of the data set, and expanding the range of applicability of the injury criterion represent substantial advancements in elucidating the

injury tolerance of the lumbar spine and further aids in the development of injury mitigation equipment, strategies, and anthropometric test devices.

Finally, the work presented in chapter 5 represents a considerable improvement over commonly used matched-pair testing for translation of human response to ATD response. By emphasizing the strain energy as the metric to match across the ATD and the human response the proposed energy method addresses the main shortcomings of a commonly used matched-pair translation by accounting for the material and behavior differences across biological components and ATDs. A key shortcoming that is addressed is the capability of the dummy to respond beyond the cadaver injury point, which inevitably shifts the injury risk assessment to the right and results in less conservative injury thresholds effectively resulting in equipment, tools, or techniques that provide less protection to the seated occupant.

6.2 Future work

While this dissertation has provided novel and significant contributions to elucidate the injury risk of the lumbar spine under dynamic compression, much work needs to be done to fully capture the complex response of the human spine during underbody blast events. This work was limited to a range of specified seated postures which bounded the contributions of bending moment to the loading event, and further confined the critical values of the combined injury metric. Ideally separate experiments that result in pure bending moment and pure axial loading respectively, should be

conducted to determine the critical values of the combined loading metric for the human lumbar spine. Moreover, the presence of supported torso mass above the lumbar spine and the common appearance of torsional and lateral bending in current military vehicles merit the expansion of the proposed injury criterion to include injury thresholds for these scenarios. Additionally, the proposed injury criteria throughout this dissertation are limited to single or multiple vertebral body fractures. Hence criteria that investigates different injury types, such as posterior element injuries, soft tissues disruptions, etc., should be developed to better represent the injury risk a seated occupant is exposed to during an UBB event.

Another direction that could be investigated addresses the age of the population studied in this dissertation. To provide an injury risk that is more representative of the military population, scaling relationships could be proposed from differences in bone mineral density, and morphology across the specimens used in this study and a younger, healthier population.

Finally, while the methodology of the proposed iso-energy translation is outlined in Chapter 5, an illustration on how the method works can be useful for its introduction to the literature. This could be achieved by a theoretical translation that uses a generic beam response as the translation target. Further, an experimental translation across cadaver response and ATD (or a surrogate) would optimally illustrate the application of the energy method.

Appendix A

Table A.-1: Input conditions and injury description summary for cadaver tests used in L_{ic} and CL_{ic} generation. "N," "PF", "PE", and "NR" denote nominal, pre-flexed, pre-extended, and not reported respectively

Test ID	Posture	Velocity (m/s)	TTP (ms)	Vert fx	Injury description
LSPN1	N	0.7	9.3	1	L1 vertebral body burst fx
LSPN2	N	2.0	10.2	1	L1 anterior vertebral body fx, L3 spinous process fx
LSPN3	N	2.8	12.2	1	L3 & L4 anterior vertebral body fx
LSPN4	NF	1.3	8.0	0	No injury
LSPN5	NF	1.0	8.3	0	L1 inf R facet fx; L1-L2 IVD ant rupture; L3-L4 IVD post rupture; L4-L5 IVD NP rupture
LSPN6	NF	2.0	12.0	0	L1 inferior left facet fx
LSPN7	NF	1.2	10.6	1	L1; L3 post crush fx; L3 L&R sup facet fx; L5 L sup facet fx; osteophyte fx L5 R inf facet; IVD rupture L2-L3 & L4-L5
LSPN8	NF	1.8	12.0	0	L3, L4 spinous process fx; L4 sup endplate fx
LSPN9	NF	2.7	12.8	0	L1 spinous process fx; L4,L5 endplate failures; T12-L1 IVD tear
LSPN10	NE	5.8	20.8	1	L1 anterior vertebral body fx, L1 bilateral transverse process fx; L1-L2 IVD NP rupture; L2 anterior vertebral body fx, L2 left superior articular process fracture, L2 ALL rupture; L3 spinous process fx; L3-L4 IVD failure; L4 bilateral pedicle fx; L5 bilateral pedicle fx
LSPN11	NE	3.9	22.6	1	L1 vertebral body burst fx, L1 bilateral pedicle fx, L1 inferior left capsular ligament rupture; L2 superior right facet fx, L2 spinous process fx; L4 spinous process fx, L4 bilateral pedicle fx; L5 superior left articular process fx, L5 left pedicle fx
LSPN12	NE	2.9	24.2	0	L2 superior endplate fx; L3 spinous process fx, L3 minor superior endplate fx; S1 vertebral body fx, bilateral fx of sacrum ala
LSPN13	NE	4.9	25.2	1	L1 vertebral body fx, L1 bilateral pedicle fx; L2 spinous process fx
LSPN14	NF	5.7	24.1	1	L2 vertebral body burst
LSPN15	NE	3.7	22.0	0	L3-L4 disc disruption; L4 spinous process fx; L5 spinous process fx; S1 vertebral body fx

Test ID	Posture	Velocity (m/s)	TTP (ms)	Vert fx	Injury description
LSPN16	NF	8.6	31.0	1	L1, L2 vertebral body crush
LSPN17	NE	3.3	19.3	1	L1 vertebral body burst fx, L1 bilateral pedicle fx, L1 spinous process fx; L2 spinous process fx
LSPN18	NF	4.8	19.6	1	L1 Vertebral body burst
LSPN19	NE	5.7	29.0	1	L3 anterior vertebral body fx, L3 spinous process fx
LSPN20	NF	7.5	29.7	1	T12 vertebral body fx; L1 vertebral body crush; L1 bilateral lamina fx; L2 vertebral body crush
LSPN21	NE	3.4	18.0	0	No injuries to the lumbar spine. T12 vertebral body burst fx
LSPN22	NF	2.5	17.8	1	L1 Vertebral body fx; S1 compression fx
LSPN23	NE	6.4	30.7	1	L1 vertebral body burst. T12 vertebral body burst fx, S1 body fracture
LSPN24	NF	5.6	28.5	1	T12 Vertebral body fx; L1 vertebral body fx; L5 left transverse process and left inferior articular facet fx; S1 compression fx
LSPN25	NF	3.9	18.2	1	T12 vertebral body fx; L1 vertebral body fx
LSPN26	NF	4.7	27.6	1	T12 vertebral body fx; L1 vertebral body crush; S1 fx
LSPN27	NF	2.9	17.7	1	L1 vertebral body burst; L2 minor endplate failure; L3 vertebral body fx; L5 minor endplate failure
LSPN28	NF	7.3	29.7	1	L1 burst fx; L2 burst fx; L1 superior left facet fx; L2/L3 bilateral capsular ligament rupture; L5 minor inferior endplate failure with NP intrusion
LSPN29	NE	2.9	18.0	1	L1 vertebral body fx.
LSPN30	NE	4.0	28.4	1	L2 bilateral pedicle fx; L3 vertebral body wedge fx, L3 right superior facet fx, L3 spinous process fx
LSPN31	NE	3.8	18.3	1	L1 vertebral body burst fx, L1 right transverse process fx at proximal end; L2 spinous process fx
LSPN32	NE	7.7	30.2	1	T12 inferior endplate fx, L1 vertebral body burst fx, L2 vertebral body fx, L3 spinous process fx, L4 bilateral pedicle fx, L5 bilateral pedicle fx
VCLM030	N	4.3	7.2	1	L1 burst fx; posterior column involvement; retropulsion of posterior body (middle column) into spinal canal
VCLM038	N	3.2	8.1	1	L1 superior endplate fx

Test ID	Posture	Velocity (m/s)	TTP (ms)	Vert fx	Injury description
VCLM045	N	4.1	8.1	1	L1 compression fx
VCLM053	N	2.5	5.4	1	L1 compression fx
VCLM066	N	7.5	9.8	1	L1 burst fx with retropulsion into spinal canal
VCLM081	N	9.0	4.5	1	L1 Burst Fx w/ retropulsion, post elements unaffected; L2 Burst Fx; L2 Left Superior Articular Process Fx; L3 Right Superior Articular Process Fx; L3,L4 Spinous Process Fx; S1 Superior Articular Process/Facet (right); S1 Sacral Ala Fx (left)
VCLM133	N	NR	NR	0	L1 Superior Endplate Fx
VCLM229	N	7.2	19.3	1	L1 burst fracture with posterior element involvement; L1 pars fx (left), L1 pedicle fx (bilateral); L2 superior endplate fx
VCLM272	N	5.7	17.1	1	L1 burst Fracture w/ canal retropulsion
VCLM295	N	3.8	5.9	0	L3 burst fx w/ minimal retropulsion of posterior VB into spinal canal as evidenced by intact PLL
VCLM301	N	8.9	2.7	1	L1 burst, L3vb, L4ep
VCLM303	N	8.3	6	1	L1ep, L3 burst, L3-4post
VCLM305	N	7.6	10.7	1	L1comp, L2burst, L4comp, L5comp
VCLM307	N	6.2	2.3	0	Non-injury
VCLM309	N	5.7	12.4	1	L1vb,ep,post, L2burst, L1-2post
VCLM310	N	2.7	4.3	1	L1 Compression Fx
VCLM311	N	2.8	4.4	1	L1 Compression Fx
VCLM313	N	5.8	4.2	1	L1 Fracture at anterior middle column; L1 Posterior ligament disruption; T12-L1 Facet dislocation at posterior column
VCLM315	N	5.2	4.5	1	L1 Compression fracture with superior and inferior endplate involvement; T12 Endplate fracture
VCLM317	N	8.4	10.6	1	L1burst, L2burst, L3post, L1-2post, L2-3post
VCLM318	N	3.7	5.6	0	T12comp,ep,post, T12-L1
VCLM320	N	3.6	19.5	1	L2 Compression fracture with superior endplate involvement
VCLM322	N	7.8	3.8	1	T12vb, T12-L1post, L1burst, L1-2post, L2post, L3post, L3-4post, L4post, L4-5post, L5post
VCLM324	N	4.1	2.6	1	Multi-level Severe Fx

Test ID	Posture	Velocity (m/s)	TTP (ms)	Vert fx	Injury description
VCLM326	N	5.5	2.8	1	L1 Compression fracture with superior endplate involvement; T12 Inferior endplate fracture
VCLM328	N	6.1	3	1	L1 Burst fracture with retropulsion; T12 Inferior endplate fracture
VCLM330	N	8.4	3.8	1	L1post, L1-2, L2burst, L3vb, post, L3-4post, L4vb, post, L5post
VCLM333	N	6.4	2.9	1	T12-L1, L1comp, ep, L1-2, L2comp, ep, L2-3, L5avul, S1trans
VCLM335	N	5.4	2.6	1	L2 Compression fracture with superior and inferior endplate involvement; L1-L2 Disc disruption; T12 Inferior endplate fracture
VCLM337	N	4.8	2.5	1	L2 Compression fracture with superior endplate involvement; L1-L2 Disc disruption
VCLM339	N	4.5	3.6	1	T12-L1, L1comp, L1-2, L2comp
VCLM341	N	7.1	2.9	1	T12-L1, L1burst, L1-2post, L3post, S1ep
VCLM343	N	7.6	3.5	1	T12-L1, L1comp-2, L2comp, ep, L3ep, L5comp, ep, S1ep
VCLM345	N	6.4	2.8	1	L2 Compression fracture with superior and inferior endplate involvement
VCLM347	N	6.5	11.7	1	T12-L1, L1-2, L1comp, ep, post, L1-2, L2comp, ep, post, L2-3post
VCLM349	N	12.3	9.4	1	L1burst, L1-2post, L2vb, post, L4trans, L5post, S1trans
VCLM351	N	10.6	8.8	1	T12vb, T12-L1, L1vb, L2vb, L3post, L4post, S1-2trans
VCLM353	N	8.9	6.2	1	L2burst, L2-3post
VCLM355	N	7.7	10	1	L1 Involvement
VCLM357	N	5.1	17.5	1	T12, S1 Fractures- T12 within potting, S1 near screw stabilization
VCLM359	N	5.5	18	1	L1, L2 involvement
VCLM361	N	5.1	21	1	L1 inferior endplate
VCLM363	N	9.4	6	1	L1 burst, L2 Burst, L3 VB Fx, S1 Body Fx

Table A-2: Summary of combined F_z, M_y, and F_r based peak values from Duke and MCW thoracolumbar data set for L_{ic} and CL_{ic} generation. All metric values are translated to the center of the T12-L1 IVD and correspond to the injury test. "N", "PF", and "PE" denote nominal, pre-flexed, and pre-extended testing postures respectively. Non-vertebral body fracture test values for acoustic and strain gauge fracture identification are denoted with "-". For specimens that presented vertebral body fractures, the maximum value for each metric was used as the upper bound of the censored interval and the acoustic and strain gauge injury onset was used as the lower bound of the censored interval. Specimens that did not present vertebral body fractures were categorized as right censored with the maximum value of each metric.

Test	Posture	Maximum Value						Acoustic and Strain Gauge Injury Onset						Vertebral body fracture
		F_z (N)	M_y (Nm)	F_x (N)	F_r (N)	F_z/M_y κ	F_r/M_y κ	F_z (N)	M_y (Nm)	F_x (N)	F_r (N)	F_z/M_y κ	F_r/M_y κ	
LSPN1	N	2474	14	681	2566	0.41	0.43	704	10	54	706	0.12	0.12	1
LSPN2	N	6447	75	286	6453	1.11	1.11	6066	28	560	6092	1.01	1.01	1
LSPN3	N	7945	33	1157	8028	1.31	1.33	1754	7	87	1756	0.29	0.29	1
LSPN4	PF	5692	134	-78	5692	1.03	1.03	-	-	-	-	-	-	0
LSPN5	PF	4302	99	70	4302	0.78	0.78	-	-	-	-	-	-	0
LSPN6	PF	5854	44	-1339	6006	0.98	1.01	-	-	-	-	-	-	0
LSPN7	PF	3635	67	-1118	3802	0.64	0.67	2464	1	583	2484	0.40	0.40	1
LSPN8	PF	4766	57	-525	4795	0.82	0.82	-	-	-	-	-	-	0
LSPN9	PF	7516	52	-684	7548	1.26	1.27	-	-	-	-	-	-	0
LSPN10	PE	7677	28	196	7680	1.27	1.27	1621	30	17	1621	0.29	0.29	1
LSPN11	PE	5872	69	-715	5915	1.01	1.01	4272	273	43	4293	0.92	0.92	1
LSPN12	PE	4005	15	1383	4237	0.66	0.70	-	-	-	-	-	-	0
LSPN13	PE	5753	104	511	5776	1.02	1.02	1053	118	93	1057	0.27	0.27	1
LSPN14	PF	6633	242	62	6633	1.27	1.27	2482	34	162	2483	0.43	0.43	1
LSPN15	PE	5211	29	-253	5217	0.87	0.87	-	-	-	-	-	-	0
LSPN16	PF	7442	4	-2411	7822	1.21	1.27	2089	5	1245	2141	0.34	0.35	1
LSPN17	PE	5089	55	697	5137	0.87	0.88	1091	101	123	1098	0.26	0.26	1

LSPN18	PF	7680	124	106	7681	1.35	1.35	2070	23	727	2080	0.35	0.36	1
LSPN19	PE	6585	68	436	6600	1.12	1.13	661	108	173	668	0.20	0.20	1
LSPN20	PF	7316	35	-1840	7544	1.21	1.25	1543	69	946	1558	0.31	0.31	1
LSPN21	PE	7201	9	-641	7230	1.17	1.18	-	-	-	-	-	-	0
LSPN22	PF	5199	48	-885	5274	0.88	0.89	1283	4	218	1301	0.21	0.21	1
LSPN23	PE	5766	1	-675	5805	0.94	0.94	1291	73	6	1291	0.27	0.27	1
LSPN24	PF	5444	3	-1632	5684	0.88	0.92	1415	6	629	1451	0.23	0.24	1
LSPN25	PF	6705	12	-791	6752	1.10	1.10	1210	48	994	1236	0.24	0.24	1
LSPN26	PF	6335	40	119	6336	1.06	1.06	850	13	168	867	0.15	0.15	1
LSPN27	PF	4777	35	-442	4798	0.80	0.81	1353	12	474	1361	0.23	0.23	1
LSPN28	PF	7754	488	-1159	7840	1.66	1.67	2387	127	279	2403	0.49	0.49	1
LSPN29	PE	5208	40	445	5226	0.88	0.88	997	21	349	998	0.18	0.18	1
LSPN30	PE	4379	86	464	4404	0.78	0.78	518	13	70	523	0.09	0.10	1
LSPN31	PE	7201	36	315	7208	1.20	1.20	1542	14	379	1544	0.26	0.26	1
LSPN32	PE	7507	396	500	7523	1.54	1.54	754	50	330	762	0.16	0.16	1
VCLM030	N	11818	59	2244	12029	1.96	2.00	848	3	189	869	0.14	0.14	1
VCLM038	N	5846	47	216	5850	0.99	0.99	5589	33	1615	5817	0.93	0.97	1
VCLM045	N	6814	23	1674	7017	1.12	1.16	6089	5	1231	6213	0.99	1.01	1
VCLM053	N	4982	4	806	5047	0.81	0.82	4929	5	783	4991	0.80	0.81	1
VCLM066	N	9436	261	3817	10179	1.74	1.86	8383	335	3851	9225	1.63	1.77	1
VCLM081	N	5208	311	1248	5356	1.10	1.12	2203	123	1074	2451	0.46	0.50	1
VCLM133	N	1578	2	160	1586	0.26	0.26	-	-	-	-	-	-	0
VCLM229	N	6182	56	865	6242	1.05	1.06	6122	55	865	6183	1.04	1.05	1
VCLM272	N	6512	31	1936	6794	1.08	1.13	3757	29	1257	3962	0.63	0.67	1
VCLM295	N	4994	5	1077	5109	0.81	0.83	4817	5	995	4918	0.76	0.78	1
VCLM301	N	6808	105	1365	6944	1.19	1.21	5252	25	321	5262	0.87	0.87	1
VCLM303	N	9419	33	1854	9600	1.55	1.58	6654	32	1103	6745	1.10	1.12	1
VCLM305	N	7497	94	1953	7748	1.29	1.33	608	1	115	619	0.10	0.10	1
VCLM307	N	8626	76	1344	8730	1.46	1.48	-	-	-	-	-	-	0

VCLM309	N	7146	13	1846	7381	1.17	1.21	495	3	56	498	0.08	0.08	1
VCLM310	N	4504	19	982	4610	0.75	0.76	3193	32	888	3315	0.54	0.56	1
VCLM311	N	5325	57	1286	5478	0.91	0.93	5281	54	1275	5433	0.90	0.92	1
VCLM313	N	7055	317	2948	7646	1.40	1.50	5859	10	1420	6028	0.96	0.98	1
VCLM315	N	7133	13	2165	7454	1.17	1.22	7125	13	2165	7447	1.17	1.22	1
VCLM317	N	7791	1	1982	8039	1.26	1.30	4552	12	1054	4672	0.75	0.77	1
VCLM318	N	5183	89	1377	5363	0.91	0.94	-	-	-	-	-	-	0
VCLM320	N	6399	48	721	6439	1.08	1.08	250	2	55	256	0.04	0.04	1
VCLM322	N	9167	129	1415	9276	1.59	1.61	4756	12	861	4833	0.78	0.79	1
VCLM324	N	3815	180	718	3882	0.77	0.78	3432	120	1183	3630	0.65	0.69	1
VCLM326	N	5382	11	1172	5508	0.88	0.90	4781	49	1188	4926	0.82	0.84	1
VCLM328	N	4591	2	948	4687	0.75	0.76	2584	3	501	2632	0.42	0.43	1
VCLM330	N	7084	41	1373	7215	1.18	1.20	5726	7	914	5798	0.93	0.95	1
VCLM333	N	4423	8	1281	4605	0.72	0.75	4414	8	1288	4598	0.72	0.75	1
VCLM335	N	5681	35	1617	5907	0.95	0.99	5473	26	1489	5672	0.91	0.94	1
VCLM337	N	7821	1	1561	7975	1.27	1.29	7799	2	1538	7949	1.27	1.29	1
VCLM339	N	5503	94	1441	5689	0.97	1.00	4076	43	995	4196	0.70	0.72	1
VCLM341	N	8005	1	1689	8182	1.30	1.33	683	6	311	750	0.12	0.13	1
VCLM343	N	6282	73	1680	6503	1.08	1.11	3907	51	1032	4041	0.68	0.70	1
VCLM345	N	9645	28	1546	9768	1.59	1.61	9170	5	1283	9259	1.49	1.50	1
VCLM347	N	6187	48	1125	6289	1.04	1.06	4204	45	619	4249	0.72	0.73	1
VCLM349	N	12692	12	2983	13038	2.07	2.12	12638	17	3025	12995	2.06	2.12	1
VCLM351	N	5757	39	585	5786	0.96	0.97	4745	7	1116	4875	0.77	0.80	1
VCLM353	N	10233	21	2476	10528	1.68	1.72	8731	83	2553	9096	1.48	1.54	1
VCLM355	N	6148	107	1198	6264	1.08	1.10	4205	119	924	4306	0.78	0.80	1
VCLM357	N	6484	38	1707	6705	1.08	1.12	5120	29	820	5185	0.85	0.86	1
VCLM359	N	5328	23	496	5351	0.88	0.89	5040	25	552	5070	0.84	0.84	1
VCLM361	N	6798	186	19	6798	1.25	1.25	5582	93	491	5603	0.98	0.98	1
VCLM363	N	6916	125	2726	7434	1.22	1.31	4556	142	1915	4942	0.85	0.92	1

References

Anderson, T.W., Darling, D.A., 1954. A test of goodness of fit. Journal of the American statistical association 49, 765-769.

Arbogast, K.B., Maltese, M.R., 2015. Pediatric biomechanics, Accidental Injury. Springer, pp. 643-696.

Arsh, A., Darain, H., Haq, Z.U., Zeb, A., Ali, I., Ilyas, S.M., 2017. Epidemiology of spinal cord injuries due to bomb blast attacks, managed at paraplegic centre peshawar, pakistan: a nine years retrospective study. Khyber Medical University Journal 9.

Arun, M.W., Yoganandan, N., Pintar, F.A., Wolfla, C.E., Chancey, V.C., McEntire, B.J., 2014. Failure biomechanical responses of isolated and intact human thoracic spine structures. International journal of vehicle safety 7, 265-281.

Bailey, A.M., Christopher, J.J., Brozoski, F., Salzar, R.S., 2015. Post mortem human surrogate injury response of the pelvis and lower extremities to simulated underbody blast. Annals of biomedical engineering 43, 1907-1917.

Bass, C.R., Salzar, R.S., Lucas, S., Rafaels, K.A., Damon, A.M., Crandall, J.R., 2010. Re-evaluating the neck injury index (NII) using experimental PMHS tests. Traffic injury prevention 11, 194-201.

Blair, J.A., Patzkowski, J.C., Schoenfeld, A.J., Cross Rivera, J.D., Grenier, E.S., Lehman, R.A., Jr., Hsu, J.R., Skeletal Trauma Research, C., 2012. Spinal column injuries among Americans in the global war on terrorism. J Bone Joint Surg Am 94, e135(131-139).

Craig, A., Hancock, K., Dickson, H., Martin, J., Chang, E., 1990. Psychological consequences of spinal injury: A review of the literature. Australian and New Zealand Journal of Psychiatry 24, 418-425.

Cutcliffe, H.C., Schmidt, A.L., Lucas, J.E., R'Dale'Bass, C., 2012. How few? Bayesian statistics in injury biomechanics. Stapp car crash journal 56, 349.

Danelson, K., Watkins, L., Hendricks, J., Frounfelker, P., Pizzolato-Heine, K., Valentine, R., Loftis, K., 2018. Analysis of the frequency and mechanism of injury to warfighters in the under-body blast environment. SAE Technical Paper.

Danelson, K.A., Kemper, A.R., Mason, M.J., Tegtmeyer, M., Swiatkowski, S.A., Bolte IV, J.H., Hardy, W.N., 2015. Comparison of ATD to PMHS response in the under-body blast environment. SAE Technical Paper.

Duma, S.M., Kemper, A.R., McNeely, D.M., Brolinson, P.G., Matsuoka, F., 2006. Biomechanical response of the lumbar spine in dynamic compression. Biomedical sciences instrumentation 42, 476-481.

Eppinger, R., Kleinberger, M., Kuppa, S., Saul, R., Sun, E., 1998. Development of improved injury criteria for the assessment of advanced automotive restraint systems.

Foster, J., Kortge, J., Wolanin, M., 1994. Hybrid III-a biomechanically-based crash test dummy, in: Backaitis, S.H., Mertz, H.J. (Eds.), HYBRID III: THE FIRST HUMAN-LIKE CRASH TEST DUMMY. Society of Automotive Engineers, Inc., pp. 49-64.

Galante, J.O., 1967. Tensile properties of the human lumbar annulus fibrosus. Acta Orthopaedica Scandinavica 38, 1-91.

Groessl, E.J., Liu, L., Chang, D.G., Wetherell, J.L., Bormann, J.E., Atkinson, J.H., Baxi, S., Schmalzl, L., 2017. Yoga for military veterans with chronic low back pain: A randomized clinical trial. American journal of preventive medicine 53, 599-608.

Kang, D.G., Lehman, R.A., Jr., Carragee, E.J., 2012. Wartime spine injuries: understanding the improvised explosive device and biophysics of blast trauma. The Spine Journal 12, 849-857.

Kent, R.W., Funk, J.R., 2004. Data censoring and parametric distribution assignment in the development of injury risk functions from biochemical data. SAE Technical Paper.

Klein, J.P., Moeschberger, M.L., 2006. Survival analysis: techniques for censored and truncated data. Springer Science & Business Media.

Kovacs, F.M., Abraira, V., Zamora, J., del Real, M.T.G., Llobera, J., Fernández, C., 2004. Correlation between pain, disability, and quality of life in patients with common low back pain. Spine 29, 206-210.

Kuppa, S., Eppinger, R.H., McKoy, F., Nguyen, T., Pintar, F.A., Yoganandan, N., 2003. Development of side impact thoracic injury criteria and their application to the modified ES-2 dummy with rib extensions (ES-2re). SAE Technical Paper.

Loftis, K., Sandora, K., Drewry, D., 2021. Introduction to the WIAMan Biomechanics Program. Springer, pp. 1-2.

Loftis, K.L., Mazuchowski, E.L., Clouser, M.C., Gillich, P.J., 2019. Prominent injury types in vehicle underbody blast. Military medicine 184, 261-264.

Manchikanti, L., Pampati, V., Damron, K., Beyer, C., Barnhill, R., 2002. Evaluation of psychological status in chronic low back pain: comparison with general population. Pain Physician 5, 149-155.

Mertz, H., Irwin, A., Melvin, J., Stanaker, R., Beebe, M., 1989. Size, weight and biomechanical impact response requirements for adult size small female and large male dummies. SAE Technical Paper.

Mertz, H.J., Horsch, J.D., Horn, G., Lowne, R.W., 1991. Hybrid III sternal deflection associated with thoracic injury severities of occupants restrained with force-limiting shoulder belts. SAE transactions, 1108-1122.

Mertz, H.J., Prasad, P., Irwin, A.L., 1997. Injury risk curves for children and adults in frontal and rear collisions. SAE transactions, 3563-3580.

Mertz, H.J., Prasad, P., Nusholtz, G., 1996. Head injury risk assessment for forehead impacts. SAE transactions, 26-46.

Nightingale, R.W., McElhaney, J.H., Camacho, D.L., Kleinberger, M., Winkelstein, B.A., Myers, B.S., 1997. The dynamic responses of the cervical spine: buckling, end conditions, and tolerance in compressive impacts. SAE transactions, 3968-3988.

Nyquist, G., Begman, P., King, A.I., Mertz, H.J., 1980. Correlation of field injuries and GM hybrid III dummy responses for lap-shoulder belt restraint.

Ortiz-Paparoni, M., Op't Eynde, J., Kait, J., Bigler, B., Shridharani, J., Schmidt, A., Cox, C., Morino, C., Pintar, F., Yoganandan, N., 2021. The human lumbar spine during high-rate under seat loading: a combined metric injury criteria. Annals of biomedical engineering 49, 3018-3030.

Ortiz-Paparoni, M.A., Pigue, M., Cameron, R., 2020. Building a Whole Spine from Segments: Lumbar Spine Response during Dynamic Compression.

Pintar, F.A., Yoganandan, N., Sances, A., Reinartz, J., Harris, G., Larson, S.J., 1989. Kinematic and anatomical analysis of the human cervical spinal column under axial loading. SAE Technical Paper.

Poplin, G.S., McMurry, T.L., Forman, J.L., Ash, J., Parent, D.P., Craig, M.J., Song, E., Kent, R., Shaw, G., Crandall, J., 2017. Development of thoracic injury risk functions for the THOR ATD. Accident Analysis & Prevention 106, 122-130.

Possley, D.R., Blair, J.A., Schoenfeld, A.J., Lehman, R.A., Hsu, J.R., Consortium, S.T.R., 2012. Complications associated with military spine injuries. The Spine Journal 12, 756-761.

Prasad, P., Daniel, R.P., 1984. A biomechanical analysis of head, neck, and torso injuries to child surrogates due to sudden torso acceleration. SAE transactions, 784-799.

Reed, M.P., Ebert, S.M., 2013. The seated soldier study: posture and body shape in vehicle seats.

Rupp, J.D., 2015. Knee, thigh, and hip injury biomechanics, Accidental Injury. Springer, pp. 471-497.

SAE, S., 2007. J211-1 instrumentation for impact test—Part 1—Electronic instrumentation. SAE International.

Salzar, R.S., Lievers, W.B., Bailey, A.M., Crandall, J.R., 2015. Leg, foot, and ankle injury biomechanics, Accidental Injury. Springer, pp. 499-547.

Sedlin, E.D., Hirsch, C., 1966. Factors affecting the determination of the physical properties of femoral cortical bone. Acta Orthopaedica Scandinavica 37, 29-48.

Seipel, R.C., Pintar, F.A., Yoganandan, N., Boynton, M.D., 2001. Biomechanics of calcaneal fractures: a model for the motor vehicle. Clinical Orthopaedics and Related Research® 388, 218-224.

Shridharani, J.K., Bigler, B.R., Cox, C.A., Ortiz-Paparoni, M.A., Bass, C.R., Year Sensitive injury detection in the cervical spine using acoustic emission and continuous wavelet transform. In IRCOBI Conference.

Shridharani, J.K., Ortiz-Paparoni, M.A., Op't Eynde, J., Bass, C.R., 2021. Acoustic Emissions in Vertebral Cortical Shell Failure. J. Biomech., 110227.

Spurrier, E., Gibb, I., Masouros, S., Clasper, J., 2016. Identifying spinal injury patterns in underbody blast to develop mechanistic hypotheses. Spine 41, E268-E275.

Szuflita, N.S., Neal, C.J., Rosner, M.K., Frankowski, R.F., Grossman, R.G., 2016. Spine injuries sustained by US military personnel in combat are different from non-combat spine injuries. Military medicine 181, 1314-1323.

Tkaczuk, H., 1968. Tensile properties of human lumbar longitudinal ligaments. Acta Orthopaedica Scandinavica 39, 1-69.

Vasquez, K.B., Brozoski, F.T., Logsdon, K.P., Chancey, V.C., 2018. Retrospective analysis of injuries in underbody blast events: 2007–2010. Military medicine 183, 347-352.

Wolfe, P., 1969. Convergence conditions for ascent methods. SIAM review 11, 226-235.

Xia, Q., Wang, S., Kozanek, M., Passias, P., Wood, K., Li, G., 2010. In-vivo motion characteristics of lumbar vertebrae in sagittal and transverse planes. J. Biomech. 43, 1905-1909.

Yoganandan, N., Arun, M.W., Pintar, F.A., Szabo, A., 2014. Optimized lower leg injury probability curves from postmortem human subject tests under axial impacts. Traffic injury prevention 15, S151-S156.

Yoganandan, N., Arun, M.W., Stemper, B.D., Pintar, F.A., Maiman, D.J., 2013. Biomechanics of human thoracolumbar spinal column trauma from vertical impact loading. Annals of advances in automotive medicine 57, 155.

Yoganandan, N., Chirvi, S., Pintar, F.A., Uppal, H., Schlick, M., Banerjee, A., Voo, L., Merkle, A., Kleinberger, M., 2016. Foot–ankle fractures and injury probability curves from post-mortem human surrogate tests. Annals of biomedical engineering 44, 2937-2947.

Yoganandan, N., DeVogel, N., Moore, J., Pintar, F., Banerjee, A., Zhang, J., 2020a. Human lumbar spine responses from vertical loading: ranking of forces via Brier score metrics and injury risk curves. Annals of biomedical engineering 48, 79-91.

Yoganandan, N., Moore, J., DeVogel, N., Pintar, F., Banerjee, A., Baisden, J.L., Zhang, J., Loftis, K., Barnes, D., 2020b. Human lumbar spinal column injury criteria from vertical loading at the base: Applications to military environments. Journal of the Mechanical Behavior of Biomedical Materials, 103690.

Yoganandan, N., Pintar, F., Maiman, D., Cusick, J., Sances Jr, A., Walsh, P., 1996. Human head-neck biomechanics under axial tension. Medical engineering & physics 18, 289-294.

Yoganandan, N., Pintar, F.A., Schlick, M., Humm, J.R., Voo, L., Merkle, A., Kleinberger, M., 2015a. Vertical accelerator device to apply loads simulating blast environments in the military to human surrogates. J. Biomech. 48, 3534-3538.

Yoganandan, N., Stemper, B.D., Baisden, J.L., Pintar, F.A., Paskoff, G.R., Shender, B.S., 2015b. Effects of acceleration level on lumbar spine injuries in military populations. The Spine Journal 15, 1318-1324.

Biography

Maria Andreina Ortiz Paparoni was born in Caracas, Venezuela. She received her Bachelor of Science degree in Mechanical Engineering in the Universidad Simon Bolivar, Caracas, Venezuela in 2011. After receiving her undergraduate degree, she enrolled at Duke University in 2012, earning a Master of Science in Biomedical Engineering in 2014, and a PhD in Biomedical Engineering with a concentration on Injury Biomechanics in 2022. During her time at Duke, she earned the Duke University BioCoRE scholar award, the 2016 Ohio State University Injury Biomechanics Symposium student travel grant, the 2018 world congress of biomechanics student travel award, and the 2016 NFL symposium grant. Her first author publication "The Lumbar spine during high-rate under seat loading: a combined metric injury criterion" was published in Annals of Biomedical Engineering in 2021. Besides seven refereed journal and congress publications, she has presented at dozens of conferences and professional meetings.